HHS Public Access

Author manuscript

Cell Rep. Author manuscript; available in PMC 2021 August 18.

Published in final edited form as:

Cell Rep. 2021 July 20; 36(3): 109408. doi:10.1016/j.celrep.2021.109408.

Lin28 paralogs regulate lung branching morphogenesis

Jihan K. Osborne[1,2,5], **Melissa A. Kinney**[1,2,4], **Areum Han**[1,2,4], **Kemi E. Akinnola**[1,2], **Alena V. Yermalovich**[1,2], **Linda T. Vo**[1,2], **Daniel S. Pearson**[1,2], **Patricia M. Sousa**[1], **Sutheera Ratanasirintrawoot**[1,2], **Kaloyan M. Tsanov**[1,2], **Jessica Barragan**[1], **Trista E. North**[1], **Ross J. Metzger**[3], **George Q. Daley**[1,2,6,*]

[1]Division of Pediatric Hematology/Oncology, Boston Children's Hospital Boston, MA 02115, USA

[2]Department of Biological Chemistry and Molecular Pharmacology, Harvard Medical School, Boston, MA 02115, USA

[3]Department of Pediatrics (Cardiology), Stanford University School of Medicine, Stanford, CA 94305, USA

[4]These authors contributed equally

[5]Present address: Department of Pharmacology, University of Texas Southwestern Medical Center, Dallas, TX 75390, USA

[6]Lead contact

SUMMARY

The molecular mechanisms that govern the choreographed timing of organ development remain poorly understood. Our investigation of the role of the Lin28a and Lin28b paralogs during the developmental process of branching morphogenesis establishes that dysregulation of *Lin28a/b* leads to abnormal branching morphogenesis in the lung and other tissues. Additionally, we find that the Lin28 paralogs, which regulate post-transcriptional processing of both mRNAs and microRNAs (miRNAs), predominantly control mRNAs during the initial phases of lung organogenesis. Target mRNAs include *Sox2*, *Sox9*, and *Etv5*, which coordinate lung development and differentiation. Moreover, we find that functional interactions between Lin28a and *Sox9* are capable of bypassing branching defects in *Lin28a/b* mutant lungs. Here, we identify Lin28a and Lin28b as regulators of early embryonic lung development, highlighting the importance of the timing of post-transcriptional regulation of both miRNAs and mRNAs at distinct stages of organogenesis.

*Correspondence: george.daley@childrens.harvard.edu.

AUTHOR CONTRIBUTIONS

J.K.O. and G.Q.D, wrote the manuscript and R.J.M. provided expertise and helped revise the manuscript. J.K.O., K.E.A., L.T.V., A.V.Y., and D.S.P. performed experiments. T.E.N. helped revise the manuscript. S.R. and K.M.T. designed and cloned LIN28A mutants. A.H. and M.A.K. performed RNA-seq and analysis.

DECLARATION OF INTERESTS

G.Q.D. holds equity in and receives consulting fees for service on the scientific advisory board of 28/7 Therapeutics, Inc. He holds a patent on technology related to LIN28, and J.K.O., A.V.Y., and G.Q.D. have filed a provisional patent related in part to the current work.

SUPPLEMENTAL INFORMATION

Supplemental information can be found online at https://doi.org/10.1016/j.celrep.2021.109408.

Graphical abstract

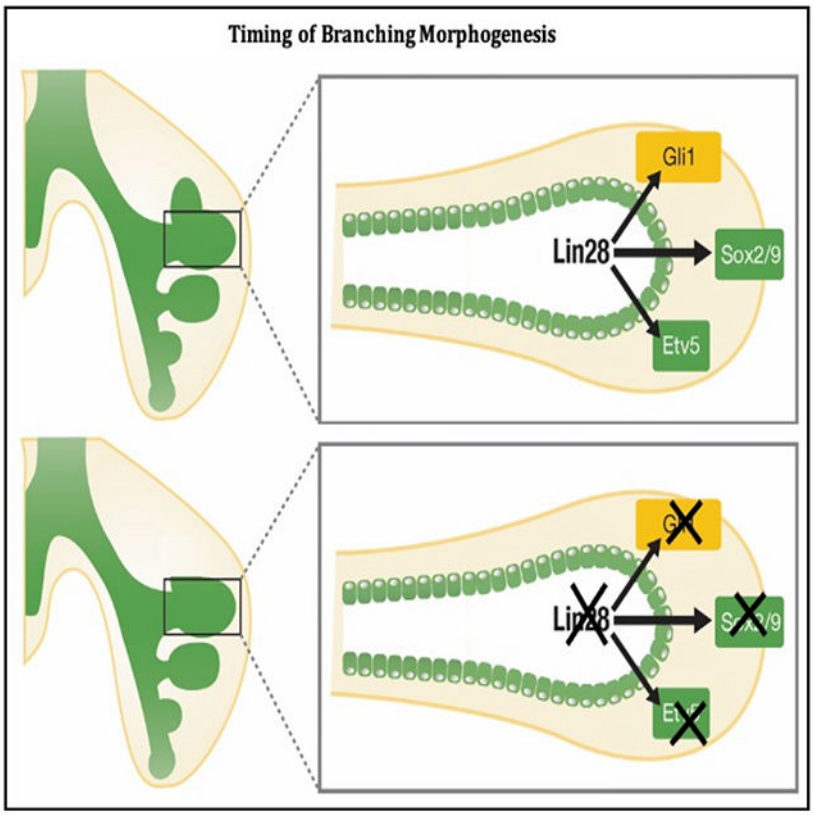

In brief

The timing of organogenesis is poorly understood. Here, Osborne et al. show that the Lin28 paralogs (Lin28a and Lin28b) regulate branching morphogenesis in a *let-7*-independent manner by directly binding to the mRNAs of *Sox2*, *Sox9*, and *Etv5* to enhance their post-transcriptional processing.

INTRODUCTION

Evolutionarily conserved heterochronic genes regulate the developmental rate and timing of metazoans from worms to mammals. The RNA-binding protein LIN-28 was one of the first heterochronic regulators identified in *Caenorhabditis elegans*, in which *lin-28* mutations at larval stage two (L2) result in either reiteration (by gain of function) or precocious maturation (by loss of function) of the hypodermal seam cells (Ambros and Horvitz, 1984; Moss et al., 1997). The mammalian paralogs Lin28a and Lin28b contribute to multiple biological processes including maintenance of pluripotency, reprogramming, and tumorigenesis by post-transcriptional regulation of both micro-RNAs (miRNAs) and mRNAs (Shyh-Chang and Daley, 2013). The developmental feedback loop between LIN28 and *let-7* is evolutionarily conserved. Early in gestation, LIN28 binds to the stem loop of *let-7* miRNA family members to inhibit their processing and subsequent expression; at later stages of development, *let-7* binds to the 3′ UTRs of the *LIN28* paralogs to suppress

their translation (Piskounova et al., 2008; Reinhart et al., 2000; Viswanathan et al., 2008). Although the LIN28 paralogs act as negative regulators of miRNAs, their association with mRNAs has been shown to increase mRNA stability and translation efficiency (Balzer et al., 2010; Polesskaya et al., 2007). In *C. elegans*, it was shown that LIN-28 regulates cell fate by the following two distinct mechanisms: the first occurs by miRNA-independent means at L2 and the second directly through *let-7* and its other family members at the larval stage two (L3) (Vadla et al., 2012).

Proper development of the mammalian lung relies on coordination of the spatial and temporal morphogenesis of epithelial progenitors to generate the airway tree. The lung epithelium is functionally divided into two divergent compartments, as follows: the bronchiolar conducting airways at the proximal regions and the alveolar sacs at the distal regions. The transcription factors Sox9 and Sox2 regulate and demarcate two waves of lung development (Alanis et al., 2014; Chang et al., 2013; Gontan et al., 2008; Tompkins et al., 2009). The first wave, marked by Sox9, produces branches that develop into both proximal and distal lineages, whereas the second wave, marked by Sox2, regulates specification of the proximal region and demarcates the bronchoalveolar junctions (Alanis et al., 2014).

Autocrine and paracrine signaling originating from both the endodermal-derived epithelium and the mesodermal-derived mesenchyme coordinate lung development (Cardoso and Lü, 2006; Herriges and Morrisey, 2014; Morrisey and Hogan, 2010). Thus, spatial expression of genes is important for delivery of the appropriate dose, duration, and transduction of signals. Crosstalk and feedback regulation between signal transduction pathways originating from the lung epithelium and mesenchyme such as Wingless-related integration 1 (WNT), (Bone morphogenetic protein) BMP, fibroblast growth factor (FGF), and Sonic Hedgehog (SHH) regulate proximal-distal patterning, branching morphogenesis, proliferation, and differentiation. Additionally, the SHH and FGF10 signaling pathways regulate branching morphogenesis through paracrine feedback loops, whereby FGF10 in the mesenchyme upregulates SHH in the epithelia and SHH feeds back to inhibit FGF10 (Bellusci et al., 1997; Chuang et al., 2003; Herriges et al., 2015; Li et al., 2005; Pepicelli et al., 1998). We and others have found that *Lin28a* and *Lin28b* are highly expressed in the embryo from the beginning of gastrulation at embryonic Day 6.5 (E6.5) through the onset of lung organogenesis from E10.5 to E18.5 (Yang and Moss, 2003). In this study, we observed that the loss or gain of *Lin28a/b* in the lung epithelium led to defects in branching morphogenesis and perinatal lethality. We present evidence that Lin28a/b coordinate branching morphogenesis in a *let-7*-independent manner, by regulation of mRNAs that are not targets of *let-7* such as *Sox2*, *Sox9*, and *Etv5*. We propose a model wherein Lin28a and Lin28b regulate branching morphogenesis by *let-7*-independent regulation of the transcription factor *Sox9*.

RESULTS

Expression of Lin28a and Lin28b in the whole embryo and mouse lung

Previously, we demonstrated that gene knockout of both *Lin28a* and *Lin28b* in the mouse results in lethality between embryonic E10.5 and E12.5 (Shinoda et al., 2013). To further understand this observation, we examined the expression patterns of both *Lin28a* and *Lin28b*

in several organs of the mouse embryo and in mouse embryonic stem cells (mESCs) by quantitative RT-PCR (qRT-PCR) and RNA *in situ* hybridization (Figures 1A and S1A–S1C). At E10.5, we found that *Lin28b*, as formerly shown for *Lin28a*, is expressed throughout the early embryo (Figure S1A); however, unlike *Lin28a* that decreased at subsequent time points of organogenesis, *Lin28b* mRNA expression persisted throughout embryogenesis (Figure 1A; Moss and Tang, 2003; Yang and Moss, 2003). We also observed that *Lin28b* mRNA expression was higher than that of *Lin28a* in the organs examined from mid-late gestation (Figure 1A). Interestingly, in the embryonic lung, we detected a wave of re-expression of the *Lin28a* mRNA and protein in late gestation that was neither previously described nor observed in other organs (Figures 1A and 1B). *Lin28a* and *Lin28b* were detected by *in situ* hybridization in both epithelium and the mesenchyme of the lung at E13.5 (annotated by the dashed lines, Figure S1B). Protein expression of Lin28a at E11.5 was observed in the epithelia (co-expressed with Nmyc, an epithelial marker) and the surrounding mesenchyme (Figure 1C; Okubo et al., 2005; Wan et al., 2005). We quantitatively analyzed the expression of the paralogs in the lung epithelial cells ($EpCAM^+$), endothelium ($CD31^+/CD45^-$), and circulating blood cells ($CD31^-/CD45^+$) and found that *Lin28a* was expressed in all fractions of wild-type lungs, whereas *Lin28b* was primarily expressed in the endothelial and circulating blood fractions with a lower level of expression in the epithelium (Figures 1D and S1D).

Lin28a and Lin28b are essential for branching morphogenesis and survival

To determine the necessity of *Lin28a* and *Lin28b* in the lung, we generated epithelial-specific single- and double-gene knockouts by using an *Nkx2.1creER* construct to drive the loss of loxp-flanked (floxed) *Lin28a* and *Lin28b* alleles throughout the whole lung epithelium (Minoo et al., 1999), with temporal control of the Cre recombinase mediated by administration of tamoxifen (hereafter, strains are referred to as *d*KO for the double $Lin28a^{-/-}$ and $Lin28b^{-/-}$ knockout, *a*KO for the single $Lin28a^{-/-}$ knockout, and *b*KO for the single $Lin28b^{-/-}$ knockout) (Taniguchi et al., 2011). For all experiments, we used tamoxifen administration at E10.5–E11 to induce *NKX2.1creER*-mediated activation or inactivation of target alleles. We determined the efficiency of Cre-mediated recombination 48-h post-tamoxifen administration by crossing the *NKX2.1creER* line to a reporter with a *floxed stop-Tdtomato* cassette and observed effective recombination throughout the whole epithelium including both tips and stalks (Figure S2A). We confirmed the loss of Lin28a by immunofluorescence. As previously noted, we observed that Lin28a was expressed in the epithelium as well as mesenchyme. Cre-mediated recombination led to a loss of Lin28a in the epithelium at 48-h post-tamoxifen administration (Figure S2B).

The mouse bronchial tree is formed by the following three distinct subroutines: domain branching, planar bifurcation, and orthogonal bifurcation (Metzger et al., 2008). We found that all three of the subroutines were used in the *a*KO and *b*KO knockouts (Figures 2 and S2). Mice with constitutive whole-body knockout of *Lin28b* alone are born normally, while constitutive whole body knockout of *Lin28a* alone results in increased perinatal lethality (Shinoda et al., 2013). We examined lungs from whole body, constitutive knockouts of either *Lin28a* alone or *Lin28b* alone, as well as the single epithelial-specific knockouts by virtue of *NKX2.1creER*. The lungs from both the whole-body and the epithelial-specific knockout

of *Lin28b* appeared normal (Figure S2C). Although we did observe smaller lungs in a small subset of the whole-body knockouts of *Lin28a* as well as with the epithelial-specific knockouts of *Lin28a*, we observed no defects that could be attributed to branching alone, as defects in lung growth and size are difficult to analyze in isolation of branching (Figure S2D).

Although the global patterning and branching subroutines were largely intact in the epithelial-specific *d*KO, we detected delayed lateral secondary branch formation and outgrowth in both left and right caudal lobes, without gross size differences (denoted with white arrows, Figures 2A, 2C, and 2E). We also observed branches with a larger diameter in several of the mutant lungs (denoted with red arrows) and increased thickness of the mesenchyme compared to the area of the whole lung across various litters at E12.5 (Figures 2A, 2C, 2G, and S2E). Subsequently, we focused on the *d*KO mutants.

Examination of *d*KO mutant lungs at later developmental stages (E14, Figure 2B; E15.5, Figures 2D and 2F) revealed phenotypes consistent with the branching delay observed at E12.5, including significantly fewer branches, as well as enlarged terminal structures. Fifty percent of the mutant lungs exhibited comparable size compared with controls, whereas the other half were significantly smaller than controls (Figure S2F). *Lin28a/b* double heterozygous mutants also demonstrated similar phenotypes, consistent with a delay in branching, including decreased lateral secondary branches and enlarged cystic terminal branches, with slight differences between the different genotypes (Figures 2I, S2G, and S2H). At early time points, we observed an increased mesenchyme area, whereas at later time points in the *d*KO lungs, we observed decreased mesenchyme relative to the whole lung area (Figures 2D and 2H). These data indicate that a precise dose of both Lin28a and Lin28b in the epithelium is required for the proper timing of lung branching morphogenesis and can influence epithelial-mesenchymal communication in the lung.

Although it has been reported that haploinsufficiency of the endogenous *NKX2.1* allele can lead to peri-natal defects (Herriges et al., 2017), in our experiments, we observed no branching defects in the single heterozygous animals harboring the *NKX2.1creER* allele in the absence of CRE induction by tamoxifen. Tamoxifen induction of *NKX2.1creER* between E10.5 and E11 caused decreased branching in only 10% (2 of the 20) of the lungs examined from strains carrying the *floxed stop-Tdtomato* cassette, *a*KO, or *b*KO alone (Figures S3C and S3D). These low-penetrance branching defects were different from those observed in the *d*KO, which manifested consistently decreased branching and dilated terminal branches at a rate of 100% (30 of the 30 *d*KO lungs examined at multiple time points).

Overexpression of *Lin28a/b* further established the requirement for precise dosing during early lung development. We examined the lungs of mice from doxycycline (dox)-inducible gain-of-function *LIN28B* (*rtTA-LIN28B*, no Cre used) and conditional gain of function (*loxp-stop-loxp-rtTA*) of both *LIN28* paralogs (i*Lin28a* and i*LIN28B*), again using the tamoxifen-induced *Nkx2.1creER* driver. Dox-inducible whole-body overexpression of LIN28B at E10.5 demonstrated larger organ size and, interestingly, thicker epithelial layers (Figure S4A). Induction of i*Lin28a* and i*LIN28B* at E10.5 likewise led to aberrant branching morphogenesis, indicated in the i*Lin28a* mutant by significantly fewer lateral secondary

branches and in both i*Lin28a* and i*LIN28B* mutants by enlarged distal tips (Figures 3A and 3B). Although both loss-of-function and gain-of-function *LIN28* affect branching, the airway epithelium of the *iLin28a* and *iLIN28B* mutants, like the constitutive mutant, appeared thicker (Figures 3C, 3D, S4A, and S4B). This overgrowth phenotype is reminiscent of previously described roles for both Lin28a and LIN28B in neoplasia (Nguyen et al., 2014; Tu et al., 2015; Urbach et al., 2014; Viswanathan et al., 2009; West et al., 2009). Notably, the similarity of the phenotype between gain and loss of function observed in our LIN28 mutants, including the appearance of enlarged termini and decreased branching, has been observed for mutants of other genes involved in branching morphogenesis, such as *Sox9* (Rockich et al., 2013).

Morphogenetic pathways are used throughout development by multiple organ systems to increase size, surface area, and complexity. To investigate further whether manipulations of *LIN28* could regulate branching morphogenesis in a second organ system, we examined the mammary gland from the dox-inducible *rtTA-LIN28B* mutant mice. Like the lung phenotype, dox induction of *LIN28B* in adult females at 3 weeks of age led to decreased branching in mammary glands (Figures S4C and S4D). These data demonstrate that precise levels of *Lin28* are required for normal branching morphogenesis in the mammary gland as well as the lung.

We also examined the effects on post-natal survival in the mutants. We found that varying deficiencies of Lin28a/b in the lung epithelium led to significant decreases in the viability of pups at birth, without decreases in body size (Tables S1 and S2; Figure S5A). Several pups failed to take a single breath, whereas others showed labored breathing before dying (Tables S1 and S2), which is consistent with a role for Lin28a and Lin28b in proper lung development.

Mature *let-7* is not expressed during early lung development

To investigate the role of the *let-7* family of miRNAs in branching morphogenesis, we conducted qRT-PCR for all eight mature *let-7* family members throughout the course of lung development. Although qualitative expression of *Let-7a* has been shown in the developing bronchial epithelium by *in situ* hybridization, we observed low expression of all individual mature *let-7* miRNAs until about E13.5 with incremental increases of *let-7a*, *let-7d*, *let-7g*, and *let-7i* until E18.5, during which time there was a decrease in expression that returned moderately during adulthood (Figures 4A, and S6A; Johnson et al., 2007). Similar to what has been shown in worms, we observed inverse patterns of expression between *Lin28a/b* and eight of the *let-7* family members, with *Lin28a/b* expression decreasing by E13.5 and *let-7* miRNAs expression commencing around E13.5 and persisting thereafter (Figure 4B and S6A). *let-7* family members in both vertebrates and invertebrates have been shown to regulate stem/progenitor cell differentiation, and thus, timing of its expression is extremely important for the coordinated exit of cells from periods of growth during organogenesis to terminal differentiation at the end of embryogenesis (Roush and Slack, 2008). To examine the functional consequences of mistimed *let-7* miRNA expression at earlier stages of lung development when Lin28a/b is present, we ectopically overexpressed *let-7S21L*, a Lin28a/b-resistant form of *let-7g*, starting at E10.5 (Figure S6B; Zhu et al., 2011). Induction

of *let-7S21L* caused abnormal branching morphogenesis with fewer branches and cystic terminal structures, phenotypically mimicking the genetic loss of Lin28a/b (Figures 4C, 4D, and 4E). *LIN28* is a known target of *let-7*, indicative of a developmental feedback loop (Pasquinelli et al., 2000; Reinhart et al., 2000; Roush and Slack, 2008; Xu et al., 2009). As expected, ectopic expression of *let-7S21L* suppressed Lin28a mRNA expression (Figure 4F). Moreover, we found that the aberrant branching caused by ectopic *let-7S21L* could be rescued by simultaneous overexpression of Lin28a (denoted with white arrows and numbers indicating lateral branches, Figures 4E and 4F). These data show that mistimed expression of *let-7S21L*, which was used here as an alternative experimental means of suppressing *Lin28a*, disrupts lung branching morphogenesis, highlighting the temporal importance of the expression of the LIN28/*let-7* axis during development.

Lin28 regulates pathways involved in branching morphogenesis

To study in an unbiased manner the potential downstream targets of LIN28/*let-7* during branching morphogenesis, we conducted RNA sequencing (RNA-seq) on whole lungs at E12.5 from control and double knockout mice. Exon mapping of *Lin28a* and *Lin28b* in three knockout samples used for RNA-seq confirmed deletion of the paralogs (Figure S7A). Comprehensively, we identified changes in 1,662 genes in the *d*KO lungs compared to controls (910 upregulated; 752 downregulated; Figure 5A). To understand pathways impacted by *Lin28a/b* ablation, we analyzed gene regulatory networks (GRNs) that were enriched in the *d*KO lungs compared to controls (Figure 5B; Cahan et al., 2014). Gene Ontology (GO) analysis of the GRNs identified transcriptional regulators involved in cell cycle and double-strand break repair to be the most decreased, and those involved in endoderm development, epithelial tube branching, and differentiation to be among the most increased (Figure 5B). Gene set enrichment analysis (GSEA) of hallmark gene sets detected dysregulation of several canonical signaling pathways known to regulate lung development, including increased expression of genes regulated by the Wnt/β-catenin and BMP signaling pathways and decreased expression of genes in the SHH and FGF pathways (Figures 5C–5F). To further analyze the genes directly regulated by the LIN28 proteins, we investigated the transcript levels of several of the mature *let-7* family members but found no increase in these mature *let-7* miRNAs in *Lin28a/b*-deficient lungs (Figure 5G). Based on this result, we next conducted an unbiased analysis of known targets of both *let-7* and Lin28a/b (Figures 5H and 5I). Of the 752 genes that were reduced in our RNA-seq data, we found 13 *let-7* targets (Figure 5I). Within this subset was downregulation of *Hmga2*, a direct target of both *let-7* and LIN28, which is known to play a role in lung proliferation and distal epithelia differentiation by enhanced WNT signaling (Hafner et al., 2013; Mayr et al., 2007; Singh et al., 2014). We next examined the direct targets of Lin28b identified from previously published *in vivo* crosslinked immunoprecipitation sequencing (CLIP-seq) data (Madison et al., 2013). Of the downregulated genes, 321 (42.6%) were direct Lin28b targets (Figures 5H and 5I). Interestingly, all but 1 of the 13 differentially expressed *let-7* targets, including *Hmga2*, were also Lin28b direct targets (Figure 5I). Moreover, several differentially expressed direct Lin28b targets are known regulators of branching morphogenesis, including *Etv5* and *Sox9* (Figure 5I). The downregulated direct targets of Lin28b were also enriched for functions in cell cycle and proliferation (Figures 5B, and 5J). Interestingly, our analysis also identified *Wnt5b*, a ligand of non-canonical Wnt signaling

that controls the cell cycle and maintains epithelial polarity during branching morphogenesis in other organs (Figure 5J; Kadzik et al., 2014; Kessenbrock et al., 2017; Li et al., 2005; Patel et al., 2011). Taken together, these results suggest that during early lung development, Lin28a and Lin28b coordinate genes specifically involved in cell cycle, proliferation, and lung branching morphogenesis predominantly through direct regulation of mRNAs.

Lin28a and Lin28b coordinate feedback between SHH/FGF10

To uncover the mechanisms underlying LIN28-mediated regulation of branching morphogenesis, we further explored the signaling pathways implicated by the GSEA in *Lin28a/b*-deficient lungs. The data from the double knockouts demonstrated that expression of the *Shh* ligand and its downstream effectors *Gli1* and *Gli2* were reduced, whereas the Hedgehog pathway inhibitor *HIP1* was unchanged relative to controls (Figure S7B). Moreover, expression of the FGF pathway ligands *FGF9* and *FGF10* were increased, whereas levels of the pan-receptor tyrosine kinase inhibitor *Sprouty1* and the downstream effector *Etv5* were reduced (Figure S7B). Interestingly, we also found expression levels of the transcription factors *Sox2* and *Sox9* to be dramatically decreased in the *d*KO lungs (Figure S7B). In the *a*KO, several of the genes examined in the *d*KO were also altered at various time points, including *Shh*, *Fgf10*, *Sox2*, and *Sox9*. Additionally, the majority of *let-7* family members remained largely unperturbed (Figure S7C). Together, these data identified genes downstream of the SHH and FGF signaling pathways, as well as transcription factors Sox2 and Sox9 as targets of Lin28a and Lin28b.

The SHH-FGF10 signaling pathways are particularly interesting due to known negative feedback mechanisms that regulate branching morphogenesis (Bellusci et al., 1997; Chuang et al., 2003; Pepicelli et al., 1998). Moreover, the FGF10 downstream effector Etv5 can positively regulate the *Shh* enhancer (Bhuiyan et al., 2013; Herriges et al., 2015). To investigate whether the signaling activity of FGF10 was impacted in our Lin28-deficient mice, we examined the expression and localization of the downstream targe, phosphorylated-ERK (pERK) and the downstream effector Etv5. We observed that pERK was increased in both the epithelium and mesenchyme of *Lin28a/b*-deficient lungs by almost 2-fold, which is consistent with an increase in FGF10 activity (Figures 6A and S7D). Etv5 expression was localized strictly to the nucleus in the distal epithelium of the control lungs (indicated by the white arrows), whereas its expression was decreased and not strictly localized to the nucleus in the *Lin28a/b*-deficient lungs (indicated by the yellow arrows, Figure 6B). This result is consistent with the recent finding that increased pERK in the epithelium can be observed with decreased *Etv5* expression (Herriges et al., 2015).

To examine whether regulation of these pathways by Lin28 could occur by direct binding to mRNA targets, we used whole-organ lysates to conduct RNA-immunoprecipitation (RIP) of genes in pathways previously shown to be dysregulated in our GSEA (Figure 6C). RIP-qPCR was conducted on the mRNA for the signaling ligands *Bmp4*, *Shh*, and *Fgf10* and their respective downstream effectors *Smad1*, *Gli1*, and *Etv5* across several wild-type organs known to use these pathways early during organogenesis for proliferation, branching morphogenesis, or differentiation (Figures 6C and S7E). Lin28a bound to *Etv5* mRNA in the lung, brain, kidney, and liver and to *Gli1* in the lung and brain (Figures 6C and S7E).

We did not observe binding of Lin28a to *Shh* and *Fgf10* mRNA in any of the organs tested. Although Lin28a was able to bind *Bmp4* mRNA, we did not observe a change specifically in this gene within our RNA-seq data, and interestingly, *Gli1* is solely expressed in the lung mesenchyme (Grindley et al., 1997). Thus, these data suggest that Lin28a and Lin28b coordinate lung branching morphogenesis through regulation of the feedback loop between SHH and FGF10 by direct binding to *Etv5* mRNA (Figure 6C).

Lin28a regulates expression of Sox9

Further interrogation of direct targets of Lin28 identified from the overlay of the RNA-seq and CLIP-seq datasets revealed the transcription factor Sox9. *Sox9* is an interesting candidate because, like Etv5, it is activated downstream of the FGF10 pathway in lung epithelia. Furthermore, Sox2 and Sox9 demarcate and regulate proximal and distal lung epithelial compartments, respectively (Alanis et al., 2014; Chang et al., 2013; Gontan et al., 2008; Hashimoto et al., 2012; Que et al., 2009; Rockich et al., 2013; Tompkins et al., 2009). Lungs deficient for both *Lin28a/b* as well as *Lin28a* alone in the epithelium have significantly decreased *Sox2* and *Sox9* mRNA (Figures S7B and S7C). We then imaged the *d*KO lungs by whole-mount immunofluorescence staining for Sox2 and Sox9 to visualize any defects in proximal and distal compartmentalization. Mutant lungs with branching defects retained normal proximal and distal compartment boundaries (Figure 6D). Consistent with mRNA expression, we observed a greater than 40% decrease in Sox2 and Sox9 protein expression in the epithelium of the mutant lungs as compared to controls (Figures 6D and S7F). To test whether regulation of *Sox2* and *Sox9* occurred by mRNA binding, we performed RIP-qPCRs in various organs shown to express Lin28 and found that Lin28a was able to bind directly to both *Sox2* and *Sox9* in the heart, lung, brain, and kidney but not the liver (Figures 6E and 6F). Next, we wanted to understand whether the decrease we observed was due to less Sox2 and/or Sox9 expressed in the whole lung or a decrease in Sox2 and/or Sox9 expression at the single-cell level. To answer this question, we performed immunofluorescence on serial sections of control and double-knockout lungs and counted the number of Sox2- and Sox9-positive cells. We observed fewer Sox2- and Sox9-positive cells in the double-knockout lungs that those in the control rather than an overall decrease in the expression of Sox2 and Sox9 throughout the whole lung (Figures 6G and 6H). Thus, the decrease in the *dKO* mutant of the total amount of Sox2 and Sox9 protein expression is consistent with there being fewer epithelial cells expressing Sox2 and Sox9. Taken together, the data suggest that Lin28a and Lin28b are capable of regulating lung development through binding and regulating *Sox2* and *Sox9* mRNA.

Previous reports of a loss of Sox9 in the epithelia by using a *ShhCre* noted defects in both branching morphogenesis and alveolar differentiation (Chang et al., 2013; Rockich et al., 2013). We have demonstrated that overexpression of both LIN28 paralogs leads to decreased branching and enlarged distal tips (Figures 3A and 3B). Interestingly, induction of *Lin28a* in the epithelium leads to increased expression of *Nmyc* and *Sox9* but not *Sox2*; thus, we focused primarily on the regulation of *Sox9* (Figure 7A). Because we established that *Sox9* is a potential direct target of LIN28 in the lung (Figure 6F) and overexpression of *Lin28a* leads to increased *Sox9* expression (Figure 7A), we next investigated whether a heterozygous loss of *Sox9* (using *NKX2.1creER*) could rescue branching defects or the

enlarged distal tips observed in the *iLin28a* mutant. Indeed, we found that a heterozygous loss of *Sox9* could rescue the enlarged distal tip phenotype but not the branching defects (Figure 7B). Additionally, we confirmed that overexpression of *Lin28a* in the heterozygous *Sox9* mutant rescued mRNA expression of *Sox9* but not *Sox2* (Figure 7C). LIN28A and LIN28B have been shown to directly control mRNA processing and translation efficiency independent of *let-7* regulation (Cho et al., 2012; Tan et al., 2014, 2019; Wilbert et al., 2012). To further understand how Lin28a regulates Sox9 expression, we examined the mRNA half-life of *Sox9*, hypothesizing that these interactions would result in an increased mRNA half-life. Because we demonstrated that Lin28a was able to bind to *Sox9* mRNA in the embryonic kidney at E13 (Figure 6F), during the onset of kidney branching (Costantini and Kopan, 2010), we expressed a GFP control, wild-type human LIN28A, or a human mRNA-binding mutant of LIN28A together with *Sox9* in human embryonic kidney cells (which express neither *Sox9* nor LIN28A). Overexpression of wild-type LIN28A led to a 6-fold increase in mRNA half-life of *Sox9* as compared to the mRNA-binding mutant, and a 3-fold increase compared to the GFP control (Figures 7D and 7E). Taken together, these findings suggest that Lin28a in part controls branching morphogenesis by direct regulation of *Sox9* mRNA stability.

DISCUSSION

Mammalian organogenesis relies on the interaction of complex signaling pathways and their downstream effectors to ensure accurate timing of stem/progenitor cell self-renewal, proliferation, and differentiation. These signaling pathways entail elaborate feedback and crosstalk mechanisms to achieve the appropriate timing of morphogenic events. Here, we describe a role for LIN28-mediated post-transcriptional regulation of mRNAs involved in several signaling pathways during lung branching morphogenesis.

At early time points, the delay in branch formation observed with Lin28 deficiency is reminiscent of a delay in development similar to the heterochronic phenotype observed in worms with the loss of LIN-28 (Ambros and Horvitz, 1984). In addition to the lung, we found that manipulations of Lin28a/b in the mammary gland caused branching defects. Similarly, we have recently published data showing a role for Lin28b during kidney branching morphogenesis (Yermalovich et al., 2019), suggesting a broader role for the LIN28 paralogs in branching morphogenesis of multiple organs. Contrary to what was observed in the overexpression mutant of LIN-28 in the worm, we found a decrease in lung branching morphogenesis similar to the epithelial knockout, suggesting that precise doses of Lin28a and Lin28b are required for proper organogenesis. Although roles for Lin28a, Lin28b, and *let-7* have been investigated in the stem/progenitor cells of mammalian neural lineages, other cells and tissues analogous to worm hypodermal seam cells such as the lungs and skin have not been extensively studied (Balzer et al., 2010; Nishino et al., 2013; Rybak et al., 2008; West et al., 2009). A recent finding also suggested a role for Lin28a overexpression at later time points during lung development, implying effects on differentiation (Komarovsky Gulman et al., 2019).

The phenotype associated with the loss of Lin28a/b in the lung epithelium could be explained at least in part by direct regulation of the transcription factor Etv5. It has been

demonstrated that the feedback regulation to and from FGF10 and SHH is mediated by Etv5 regulation of the *Shh* enhancer (Herriges et al., 2015). Interestingly, we observed that Lin28 is capable of binding Gli1, a lung mesenchymal transcription factor, suggesting LIN28 may regulate the feedback between the SHH and FGF10 pathways in multiple compartments of the lung. Although SHH and FGF are associated with branching morphogenesis and proliferation in the lung, the signaling molecules and their downstream targets, such as Sox9 and the ETVs, are also involved in branching morphogenesis and proliferation of other organs, including the kidney, emphasizing the importance of further investigation of transcriptional and post-transcriptional regulation of these developmental signaling pathways (Chen et al., 2014; Kuure et al., 2010; Reginensi et al., 2011; Seymour et al., 2007).

We found that LIN28 is capable of binding to and controlling the expression of *Sox2* and *Sox9* by increasing mRNA stability and/or translation. Although previous reports using the *NKX2.1creER* demonstrate a mosaic pattern of recombination, we found little indication of this in our model (Chang et al., 2013). *In vivo* data from the loss-of-function, gain-of-function, rescue, and RNA-binding experiments together with the *in vitro* data from the half-life experiment suggest that *Sox9* may be a bona fide direct target of LIN28. Although several of the phenotypes suggested here could be accounted for through the direct interaction of LIN28 and *Sox9*, direct regulation of a number of other targets including *Etv5* cannot be ruled out. Several different classes of mRNAs bound by Lin28a/b are known, including cell cycle regulators, RNA-splicing factors, histones, and genes involved in glucose metabolism, but these mRNAs have also been characterized as *let-7* targets (Tsialikas and Romer-Seibert, 2015). Although our data show that the effects of Lin28 expression on early stages of lung development are largely *let-7* independent, we cannot exclude the possibility of a *let-7*-dependent role for Lin28a/b in the regulation of transcripts during later time points of lung development, when both *let-7* miRNAs and Lin28a/b are expressed. However, we find it compelling that many of the major regulators of early development and branching morphogenesis, such as *Sox9* and *Etv5*, do not contain known *let-7* binding sites and are bound by Lin28a/b in multiple organs. The findings presented here establish an early role for the LIN28 proteins during the process of lung branching morphogenesis through the post-transcriptional control of *Sox9* and potentially *Etv5* and add to our mechanistic understanding of the development of this complex organ.

STAR★METHODS

RESOURCE AVAILABILITY

Lead contact—Further information and requests for all original resources and reagents presented in this manuscript should be directed to and will be fulfilled by the Lead contact, George Q. Daley (george.daley@childrens.harvard.edu).

Materials availability—This study generated two new reagents: human pBABE-LIN28A mutant (with the cold shock domain (CSD) and the zinc knuckles domain (ZKD) mutated to abolish RNA binding capacity. These plasmids are available upon request to the Lead contact.

Data and code availability—The published article includes all datasets generated and analyzed during this study. The RNA-seq data described in this study are deposited to the Gene Expression Omnibus (GEO) repository. The accession number for the RNA-seq data reported in this paper is GEO: ID GSE93571. The previously published LIN28B CLIP data was obtained from, Madison et al., 2013. Predicted *Let-7* targets were found via TargetScan (http://www.targetscan.org/vert_72/).

EXPERIMENTAL MODEL AND SUBJECT DETAILS

Animal studies

Gene Nomenclature: *Lin28a/Lin28b* (Mouse gene-RNA/DNA); Lin28a/Lin28b (Mouse protein); *LIN28A/LIN28B* (Human gene-RNA/DNA); LIN28A/LIN28B (Human protein); Use of Lin28 or LIN28 refers to both human and mouse Lin28a/A and/or Lin28b/B ; LIN-28 (Worm protein); *lin-28* (Worm gene-RNA/DNA).

Mice: All mouse experiments were conducted in accordance with the Institutional Animal Care and Use Committee at Boston Children's Hospital that is accredited by AAALAC. Generation of the *Lin28b* knockout conditional double and single knockout, inducible *let-7S21L, Lox-stop-Lox-TetOn*- Lin28a and LIN28B mice were as previously described in Shinoda et al. (2013) and Zhu et al. (2010, 2011). The *NKX2.1*-creER (JAX no. 014552), *Lox-stop-Lox-tdTomato* (JAX no. 007914), and *Sox9* mice (JAX no. 013106) were purchased from Jackson Laboratories. The whole body *Lin28a* knockout mice were generated using male floxed *Lin28a* mice crossed to female *Ddx4-cre* (JAX no. 006954) mice, note that female *Ddx4-cre* mice can be used for global recombination; paternally inherited alleles are germ-line specific, see Jackson website for more details. The mice used in the study were embryonic ages E11.5-E18.5 (except for the *TetO-LIN28B* mice used for mammary studies). Tamoxifen (Sigma) was diluted in corn oil to 20mg/ml administered intraperitoneally at a dose of 0.068mg/g per mouse weight in grams and at E10.5-11. For inducible mice doxycycline was also administered ad lib in drinking water at a concentration of 1g/L.

Cell lines—HEK293 cells were purchased from ATCC. HEK293 cells were cultured at 37°C, 5% CO_2 atmosphere, in DMEM supplemented with 10% FBS.

METHOD DETAILS

Flow cytometry and FACS analysis—Whole lung was dissociated in collagenase/dispase (Roche 10 269 63) and stained for the following markers of lung endothelium anti-mouse, CD31 PE (Biolegend); blood cells, anti-mouse CD45 PerCP-Cyanine5.5 and (Ebioscience) epithelium cells, CD326 (EpCAM) PECy7 (Biolegend). Staining was done with 0.1- 0.5 million cells with antibody dilutions of 1:100 for 20 minutes in the dark at room temperature. Cells were sorted on the BD Aria cytometer.

Tissue preparation, immunostaining, and quantification of images—At various stages, embryos were removed from timed pregnant mice anaesthetized with ketamine/xylazine and lungs were dissected and fixed in 4% PFA (0.5% for whole mount Sox2/Sox9 staining) in PBS at 4 degrees for one hour or 10% formalin overnight.

For sectioned immunofluorescent staining, they were fixed either in PFA or formalin. Lungs fixed in formalin used for immunofluorescent staining were processed using same protocol for immunohistochemical staining as below excluding peroxidase step. Lungs were cryoprotected in PBS with 30% sucrose at 4 degrees overnight and then embedded in OCT (4583, Tissue-Tek). For sectioned immunohistochemical staining, fixed lungs were fixed then moved to 70% ethanol. The protocol for immunohistochemical staining was performed as previously published (Tu et al., 2015). For immunofluorescent staining, frozen sections at were first incubated in blocking serum (PBS with 5% normal donkey serum (Sigma), 5% BSA, and 0.5% Triton X-100) for 1 hour and then incubated with primary antibodies diluted in blocking serum 4 degrees overnight. The following day, the sections were washed with PBS three times at room temperature and then incubated with secondary antibodies and DAPI diluted in blocking serum for 1 hour at room temperature. The sections were then washed as described above and mounted with Aquamount mounting medium (18606, Polysciences). For whole-mount immunostaining, the lungs were dehydrated through a methanol/PBS gradient and bleached with 6% hydrogen peroxide in methanol overnight. The lungs were rehydrated through a methanol/PBS gradient. Lungs were then washed once in 25% methanol/PBT (PBS with 0.1% (vol/vol) Tween-20), once in 50% methanol/PBT, once in 75% methanol/PBT, and twice in 100% methanol. Dehydrated specimens were stored at −20 degrees in 100% methanol. On day 1, dehydrated lungs where rehydrated through an inverted methanol/PBT series (5 min washes in each of 75%, 50% and 25% methanol/PBT, followed by 2 × 5 min washes in PBT). Cells were then stained for Sox2 and Sox9 as previously described in Alanis et al. (2014). For quantification of Sox2+ and Sox9+ cells, a total of twelve serial slices of either control and $a^{-/-}b^{-/-};NKX2.1creER$ lungs were stained for Sox2 (green) or Sox9 (red). Using ImageJ (Schindelin et al., 2012), the fluorescent signals for each channel were integrated over selected regions of interest (lung epithelial cell layers). Integrated DAPI signals of regions where the cell density was low enough to enable cell counting were used to calculate the average signal per cell, allowing us to estimate the cell numbers of cell-dense regions and the Sox2/Sox9 mean fluorescent intensities per cell.

For mesenchyme quantification we used the negative images to take the areas of the epithelia subtracted from the area of the whole lung. For mammary glands analysis, mice with constitutive doxycycline (Dox) inducible LIN28B were at 4 weeks of age were treated with and without dox. At 6 weeks of age the fourth mammary glands were removed fixed in PFA and stained with neutral red staining.

qRT-PCR—RNA was isolated from various tissues and organs (from E12.5 to adulthood) using TRIzol (Life Technologies). For mRNA and miRNA analysis, cDNA was prepared from 2 μg RNA using miSCRIPT II RT Kit (QIAGEN). Absolute quantification PCR was performed by using DNA standards purchased from IDT for amplicons of Lin28a primers (forward- AGC TTG CAT TCC TTG GCA TGA TGG; reverse- AGG CGG TGG AGT TCA CCT TTA AGA) and Lin28b primers (forward-TTT GGC TGA GGA GGT AGA CTG CAT; reverse-ATG GAT CAG ATG TGG ACT GTG CGA). cDNA standards for Let7 molecules were as previously described in Powers et al. (2016). Linear regression analysis of the cDNA standards for *Let-7, Lin28a* and *Lin28b* qPCR cycle threshold values and total RNA per cell

values were used to calculate copies per cell for each *let-7* family member and *Lin28a* and *Lin28b*. Primers for mRNAs: *Shh, Sox2, Sox9, Bmp4, Smad1, β catenin*, and *MycN* were from BioRad (PrimePCR SYBR), primers for *FGF10, ETV5, and Gli1* were as previously described in Herriges et al. (2015).

Measurement of Sox9 mRNA Half-life—Using Lipofectamine 2000, HEK293 cells were transfected once with the following constructs: Either pBabe-GFP, human pBabe-LIN28A wild-type, or a human pBABE-LIN28A mutant (with the cold shock domain (CSD) and the zinc knuckles domain (ZKD) mutated to abolish RNA binding capacity) and Sox9 (Gift from J. Rajagopal, MGH). On the third day after transfection, 293 cells were treated with actinomycin D to stop transcription (Sigma, 10ug/mL) and collected at 0,4, and 6 hr. RNA was isolated with TRIzol and cDNA was made. mRNA half-life/ was calculated using data analysis program in GraphPad Prism (Ratnadiwakara et al., 2018). Briefly, Ct values were normalized to t = 0, mRNA abundance was calculated using $2^{(-\Delta CT)}$. mRNA decay rates were determined by non-linear regression curve fitting (one phase decay) in GraphPad Prism.

Immunoblot analysis and antibodies—Whole lungs were dissected (from E11.5 to adulthood) and lysed in RIPA buffer (50mM Tris, 150mM, NaCl, 1%NP-40, 1%Sodium deoxycholate, 0.1%SDS) with protease and phosphatase inhibitor cocktail (Thermo Scientific). Lysates were then loaded on the gel in 5x Laemmli sample buffer. Gels were run, transferred to membranes that were next blocked in 5% milk. Membranes were incubated with primary antibodies and HRP-conjugated secondary antibodies. Proteins were visualized using ECL with film. Antibodies used throughout manuscript unless otherwise specified: Lin28a (Rabbit, Cell Signaling, A177) and mouse specific Lin28b (Rabbit, Cell Signaling), α/β tubulin (Rabbit, Cell Signaling), E- cadherin (Rat, Zymed), Sox2 (Goat, Santa Cruz), Sox9 (Rabbit, Millipore, AB5535).

In situ hybridization—Probes of approximately ~450-550 base pairs for mouse Lin28a and Lin28b were designed to the coding and 3′UTR regions. Digoxigenin-labeled (DIG) antisense cRNA probes made using T7 RNA polymerase provided in the T7 *in vitro* transcription kit (AM1333). Frozen sections from wild-type CD1 mice at various ages were air-dried, washed in in PBS then acetylated in acetylation buffer (0.01% triethanolamine solution in DEPC-water with 0.125 mL of acetic anhydride to 50 mL of triethanolamine solution). Slides were permeabilized in PBT (0.1% triton in phosphate-buffered solution, PBS) for 30 minutes. Slides were washed and prehybridized for in hybridization buffer (4mL-50% dextran, 4 mL- 20X SCC, 10mL formamide, 0.4mL- 50X Denhardt's solution, 1 mL fish sperm DNA) for 2 hours. Probes were diluted in hybridization buffer (0.2ng/μl) and incubated overnight at 72 degrees. Next day slides were incubated in 0.2x SCC and then washed in PBS. Slides were blocked in 20% sheep serum diluted in TTBS (Tween 20) for one hour then incubated with anti-DIG antibody at 4 degrees overnight. Slides were washed in TTBS and color reaction performed using BM Purple (Roche).

RNA immunoprecipitation (RIP)—Organs (yolk sac, lung, heart, kidney, liver, and brains (including skulls)) were dissected from E12.75 wild-type CD1-timed pregnant mice.

Lysates were homogenized in lysis buffer (HEPES 50mM, NaCL 150mM, EDTA 20mM, Triton X-100 1%, and protease inhibitor cocktail (Roche)) on ice, then spun at 4 degrees for 15 minutes at 13K. RNaseOUT inhibitor (Invitrogen) was added to spun lysates. LIN28 (Abcam) and IgG (SantaCruz) antibodies were conjugated to magnetic Dynabeads. 100 mg of total protein was added to bead/antibody complex to IP protein/RNA complexes overnight at 4 degrees. Genes were detected using qPCR. Data analysis (ΔΔCt method) was normalized first equal nanograms of cDNA from 1% input to achieve (ΔCt), then to IgG (also normalized to input) to achieve ΔΔCt.

RNA-sequencing and analysis—Lin28a and b double knockout was achieved in the lung using tamoxifen to induce recombination of exon 2 flanked with loxP sites. Total RNA was collected using TRIzol (Invitrogen) according to the manufacturer's instructions. RNA-seq libraries were constructed following the standard protocol (The SMARTer® Ultra Low Input RNA Kit by Clontech). From the raw reads, we removed adaptor sequences using a Cutadapt tool, allowing some mismatches (the specific parameters we used were -n 2 -e 0.02 –o 15). Then, the cleaned reads were aligned to the mouse genome/transcriptome (mm10 and corresponding UCSC gene model) using TopHat2 software with the following parameters (–library-type = fr-unstranded–min-intron-length = 10–coverage-search–microexon-search–min-isoform-fraction = 0) (Kim et al., 2013). To estimate expression levels for each gene, we counted aligned reads per gene using a htseq-count tool with the following parameters (–stranded = no–idattr = gene_id -t exon -i transcript_id) (Anders et al., 2015). Transcription factor networks were defined via the CellNet (Cahan et al., 2014) global gene regulatory network (GRN) and assessed for differential regulation via Gene Set Enrichment Analysis (GSEA), as an inference-based surrogate for changes in transcriptional activity. The up- and downregulated transcription factors (FDR < 0.25) were analyzed for conserved biological functions via Gene Ontology (GO) classifications. GSEA was also conducted on Hallmark gene sets. In both cases, GSEA was run with pre-ranked gene lists based on fold changes over wild-type. Expression was further analyzed within subsets of genes selected from the TargetScan database (Agarwal et al., 2015) and previously published LIN28B CLIP data (Madison et al., 2013). The raw and analyzed data in detailed method is available through Gene Expression Omnibus (GEO) with the ID GEO: GSE93571.

QUANTIFICATION AND STATISTICAL ANALYSIS

'n' values are equal to animal number of biological replicates of each experiment (which includes number of litters examined) and the number of biological *in vitro* experiments for half-life measurement. Statistical analyses for mRNA half-life were performed by GraphPad Prism Software, decay rates were quantified by non-linear regression curve fitting (one phase decay). Statistics for double knockouts and LIN28B and Lin28a overexpression were calculated via one-way ANOVA. Statistics for RIP were compared to IgG via t test. More statistical details can be found in the figure legends. All graphs represent means ± SEM, a p value of ≤ 0.05 was considered significant (* < 0.05, ** < 0.01). Quantification and analysis of RNA-seq and its comparison to CLIP-seq and *Let-7* targets via TargetScan is detailed in Methods details.

Supplementary Material

Refer to Web version on PubMed Central for supplementary material.

ACKNOWLEDGMENTS

We would like to thank R. Grant Rowe and Deepak Jha of the Daley lab and members of the Kim lab for constructive reading of the manuscript and Thorsten Schlaeger and Trevor Bingham for help with ImageJ analysis. G.Q.D. was supported by NIH RO1GM107536 and RO1GM107536-03S1 and funds from the Boston Children's Hospital Stem Cell Program.J.K.O. was supported by a post-doctoral T32 Hematology/Oncology Training grant and the Burroughs Wellcome Fund. L.T.V. was supported by the NSF graduate research fellowship. A.V.Y. was supported by NIH F99 CA212487 predoctoral fellowship. K.M.T. was an HHMI International Student Research Fellow and a Herchel Smith Graduate Fellow.

INCLUSION AND DIVERSITY

One or more of the authors of this paper self-identifies as an underrepresented ethnic minority in science. One or more of the authors of this paper received support from a program designed to increase minority representation in science. While citing references scientifically relevant for this work, we also actively worked to promote gender balance in our reference list.

REFERENCES

Agarwal V, Bell GW, Nam JW, and Bartel DP (2015). Predicting effective microRNA target sites in mammalian mRNAs. eLife 4, e05005.

Alanis DM, Chang DR, Akiyama H, Krasnow MA, and Chen J (2014). Two nested developmental waves demarcate a compartment boundary in the mouse lung. Nat. Commun 5, 3923. [PubMed: 24879355]

Ambros V, and Horvitz HR (1984). Heterochronic mutants of the nematode Caenorhabditis elegans. Science 226, 409–416. [PubMed: 6494891]

Anders S, Pyl PT, and Huber W (2015). HTSeq—a Python framework to work with high-throughput sequencing data. Bioinformatics 31, 166–169. [PubMed: 25260700]

Balzer E, Heine C, Jiang Q, Lee VM, and Moss EG (2010). LIN28 alters cell fate succession and acts independently of the let-7 microRNA during neurogliogenesis in vitro. Development 137, 891–900. [PubMed: 20179095]

Bellusci S, Grindley J, Emoto H, Itoh N, and Hogan BL (1997). Fibroblast growth factor 10 (FGF10) and branching morphogenesis in the embryonic mouse lung. Development 124, 4867–4878. [PubMed: 9428423]

Bhuiyan MI, Lee JH, Kim SY, and Cho KO (2013). Expression of exogenous LIN28 contributes to proliferation and survival of mouse primary cortical neurons in vitro. Neuroscience 248, 448–458. [PubMed: 23806711]

Cahan P, Li H, Morris SA, Lummertz da Rocha E, Daley GQ, and Collins JJ (2014). CellNet: network biology applied to stem cell engineering. Cell 158, 903–915. [PubMed: 25126793]

Cardoso WV, and Lü J (2006). Regulation of early lung morphogenesis: questions, facts and controversies. Development 133, 1611–1624. [PubMed: 16613830]

Chang DR, Martinez Alanis D, Miller RK, Ji H, Akiyama H, McCrea PD, and Chen J (2013). Lung epithelial branching program antagonizes alveolar differentiation. Proc. Natl. Acad. Sci. USA 110, 18042–18051. [PubMed: 24058167]

Chen Z, Huang J, Liu Y, Dattilo LK, Huh SH, Ornitz D, and Beebe DC (2014). FGF signaling activates a Sox9-Sox10 pathway for the formation and branching morphogenesis of mouse ocular glands. Development 141, 2691–2701. [PubMed: 24924191]

Cho J, Chang H, Kwon SC, Kim B, Kim Y, Choe J, Ha M, Kim YK, and Kim VN (2012). LIN28A is a suppressor of ER-associated translation in embryonic stem cells. Cell 151, 765–777. [PubMed: 23102813]

Chuang PT, Kawcak T, and McMahon AP (2003). Feedback control of mammalian Hedgehog signaling by the Hedgehog-binding protein, Hip1, modulates Fgf signaling during branching morphogenesis of the lung. Genes Dev. 17, 342–347. [PubMed: 12569124]

Costantini F, and Kopan R (2010). Patterning a complex organ: branching morphogenesis and nephron segmentation in kidney development. Dev. Cell 18, 698–712. [PubMed: 20493806]

Gontan C, de Munck A, Vermeij M, Grosveld F, Tibboel D, and Rottier R (2008). Sox2 is important for two crucial processes in lung development: branching morphogenesis and epithelial cell differentiation. Dev. Biol 317, 296–309. [PubMed: 18374910]

Grindley JC, Bellusci S, Perkins D, and Hogan BL (1997). Evidence for the involvement of the Gli gene family in embryonic mouse lung development. Dev. Biol 188, 337–348. [PubMed: 9268579]

Hafner M, Max KE, Bandaru P, Morozov P, Gerstberger S, Brown M, Molina H, and Tuschl T (2013). Identification of mRNAs bound and regulated by human LIN28 proteins and molecular requirements for RNA recognition. RNA 19, 613–626. [PubMed: 23481595]

Hashimoto S, Chen H, Que J, Brockway BL, Drake JA, Snyder JC, Randell SH, and Stripp BR (2012). β-Catenin-SOX2 signaling regulates the fate of developing airway epithelium. J. Cell Sci 125, 932–942. [PubMed: 22421361]

Herriges M, and Morrisey EE (2014). Lung development: orchestrating the generation and regeneration of a complex organ. Development 141, 502–513. [PubMed: 24449833]

Herriges JC, Verheyden JM, Zhang Z, Sui P, Zhang Y, Anderson MJ, Swing DA, Zhang Y, Lewandoski M, and Sun X (2015). FGF-Regulated ETV Transcription Factors Control FGF-SHH Feedback Loop in Lung Branching. Dev. Cell 35, 322–332. [PubMed: 26555052]

Herriges MJ, Tischfield DJ, Cui Z, Morley MP, Han Y, Babu A, Li S, Lu M, Cendan I, Garcia BA, et al. (2017). The NANCI-Nkx2.1 gene duplex buffers Nkx2.1 expression to maintain lung development and homeostasis. Genes Dev. 31, 889–903. [PubMed: 28546511]

Johnson CD, Esquela-Kerscher A, Stefani G, Byrom M, Kelnar K, Ovcharenko D, Wilson M, Wang X, Shelton J, Shingara J, et al. (2007). The let-7 microRNA represses cell proliferation pathways in human cells. Cancer Res. 67, 7713–7722. [PubMed: 17699775]

Kadzik RS, Cohen ED, Morley MP, Stewart KM, Lu MM, and Morrisey EE (2014). Wnt ligand/Frizzled 2 receptor signaling regulates tube shape and branch-point formation in the lung through control of epithelial cell shape. Proc. Natl. Acad. Sci. USA 111, 12444–12449. [PubMed: 25114215]

Kessenbrock K, Smith P, Steenbeek SC, Pervolarakis N, Kumar R, Minami Y, Goga A, Hinck L, and Werb Z (2017). Diverse regulation of mammary epithelial growth and branching morphogenesis through noncanonical Wnt signaling. Proc. Natl. Acad. Sci. USA 114, 3121–3126. [PubMed: 28270600]

Kim D, Pertea G, Trapnell C, Pimentel H, Kelley R, and Salzberg SL (2013). TopHat2: accurate alignment of transcriptomes in the presence of insertions, deletions and gene fusions. Genome Biol. 14, R36. [PubMed: 23618408]

Komarovsky Gulman N, Armon L, Shalit T, and Urbach A (2019). Heterochronic regulation of lung development *via* the Lin28-Let-7 pathway. FASEB J. 33, 12008–12018. [PubMed: 31373834]

Kuure S, Chi X, Lu B, and Costantini F (2010). The transcription factors Etv4 and Etv5 mediate formation of the ureteric bud tip domain during kidney development. Development 137, 1975–1979. [PubMed: 20463033]

Li C, Hu L, Xiao J, Chen H, Li JT, Bellusci S, Delanghe S, and Minoo P (2005). Wnt5a regulates Shh and Fgf10 signaling during lung development. Dev. Biol 287, 86–97. [PubMed: 16169547]

Madison BB, Liu Q, Zhong X, Hahn CM, Lin N, Emmett MJ, Stanger BZ, Lee JS, and Rustgi AK (2013). LIN28B promotes growth and tumorigenesis of the intestinal epithelium via Let-7. Genes Dev. 27, 2233–2245. [PubMed: 24142874]

Mayr C, Hemann MT, and Bartel DP (2007). Disrupting the pairing between let-7 and Hmga2 enhances oncogenic transformation. Science 315, 1576–1579. [PubMed: 17322030]

Metzger RJ, Klein OD, Martin GR, and Krasnow MA (2008). The branching programme of mouse lung development. Nature 453, 745–750. [PubMed: 18463632]

Minoo P, Su G, Drum H, Bringas P, and Kimura S (1999). Defects in tracheoesophageal and lung morphogenesis in Nkx2.1(−/−) mouse embryos. Dev. Biol 209, 60–71. [PubMed: 10208743]

Morrisey EE, and Hogan BL (2010). Preparing for the first breath: genetic and cellular mechanisms in lung development. Dev. Cell 18, 8–23. [PubMed: 20152174]

Moss EG, and Tang L (2003). Conservation of the heterochronic regulator Lin-28, its developmental expression and microRNA complementary sites. Dev. Biol 258, 432–442. [PubMed: 12798299]

Moss EG, Lee RC, and Ambros V (1997). The cold shock domain protein LIN-28 controls developmental timing in C. elegans and is regulated by the lin-4 RNA. Cell 88, 637–646. [PubMed: 9054503]

Nguyen LH, Robinton DA, Seligson MT, Wu L, Li L, Rakheja D, Comerford SA, Ramezani S, Sun X, Parikh MS, et al. (2014). Lin28b is sufficient to drive liver cancer and necessary for its maintenance in murine models. Cancer Cell 26, 248–261. [PubMed: 25117712]

Nishino J, Kim S, Zhu Y, Zhu H, and Morrison SJ (2013). A network of heterochronic genes including Imp1 regulates temporal changes in stem cell properties. eLife 2, e00924. [PubMed: 24192035]

Okubo T, Knoepfler PS, Eisenman RN, and Hogan BL (2005). Nmyc plays an essential role during lung development as a dosage-sensitive regulator of progenitor cell proliferation and differentiation. Development 132, 1363–1374. [PubMed: 15716345]

Pasquinelli AE, Reinhart BJ, Slack F, Martindale MQ, Kuroda MI, Maller B, Hayward DC, Ball EE, Degnan B, Müller P, et al. (2000). Conservation of the sequence and temporal expression of let-7 heterochronic regulatory RNA. Nature 408, 86–89. [PubMed: 11081512]

Patel N, Sharpe PT, and Miletich I (2011). Coordination of epithelial branching and salivary gland lumen formation by Wnt and FGF signals. Dev. Biol 358, 156–167. [PubMed: 21806977]

Pepicelli CV, Lewis PM, and McMahon AP (1998). Sonic hedgehog regulates branching morphogenesis in the mammalian lung. Curr. Biol 8, 1083–1086. [PubMed: 9768363]

Piskounova E, Viswanathan SR, Janas M, LaPierre RJ, Daley GQ, Sliz P, and Gregory RI (2008). Determinants of microRNA processing inhibition by the developmentally regulated RNA-binding protein Lin28. J. Biol. Chem 283, 21310–21314. [PubMed: 18550544]

Polesskaya A, Cuvellier S, Naguibneva I, Duquet A, Moss EG, and Harel-Bellan A (2007). Lin-28 binds IGF-2 mRNA and participates in skeletal myogenesis by increasing translation efficiency. Genes Dev. 21, 1125–1138. [PubMed: 17473174]

Powers JT, Tsanov KM, Pearson DS, Roels F, Spina CS, Ebright R, Seligson M, de Soysa Y, Cahan P, Theißen J, et al. (2016). Multiple mechanisms disrupt the let-7 microRNA family in neuroblastoma. Nature 535, 246–251. [PubMed: 27383785]

Que J, Luo X, Schwartz RJ, and Hogan BL (2009). Multiple roles for Sox2 in the developing and adult mouse trachea. Development 136, 1899–1907. [PubMed: 19403656]

Ratnadiwakara M, Archer SK, Dent CI, Ruiz De Los Mozos I, Beilharz TH, Knaupp AS, Nefzger CM, Polo JM, and Anko ML (2018). SRSF3 promotes pluripotency through *Nanog* mRNA export and coordination of the pluripotency gene expression program. eLife 7, e37419. [PubMed: 29741478]

Reginensi A, Clarkson M, Neirijnck Y, Lu B, Ohyama T, Groves AK, Sock E, Wegner M, Costantini F, Chaboissier MC, and Schedl A (2011). SOX9 controls epithelial branching by activating RET effector genes during kidney development. Hum. Mol. Genet 20, 1143–1153. [PubMed: 21212101]

Reinhart BJ, Slack FJ, Basson M, Pasquinelli AE, Bettinger JC, Rougvie AE, Horvitz HR, and Ruvkun G (2000). The 21-nucleotide let-7 RNA regulates developmental timing in Caenorhabditis elegans. Nature 403, 901–906. [PubMed: 10706289]

Rockich BE, Hrycaj SM, Shih HP, Nagy MS, Ferguson MA, Kopp JL, Sander M, Wellik DM, and Spence JR (2013). Sox9 plays multiple roles in the lung epithelium during branching morphogenesis. Proc. Natl. Acad. Sci. USA 110, E4456–E4464. [PubMed: 24191021]

Roush S, and Slack FJ (2008). The let-7 family of microRNAs. Trends Cell Biol. 18, 505–516. [PubMed: 18774294]

Rybak A, Fuchs H, Smirnova L, Brandt C, Pohl EE, Nitsch R, and Wulczyn FG (2008). A feedback loop comprising lin-28 and let-7 controls pre-let-7 maturation during neural stem-cell commitment. Nat. Cell Biol 10, 987–993. [PubMed: 18604195]

Schindelin J, Arganda-Carreras I, Frise E, Kaynig V, Longair M, Pietzsch T, Preibisch S, Rueden C, Saalfeld S, Schmid B, et al. (2012). Fiji: an open-source platform for biological-image analysis. Nat. Methods 9, 676–682. [PubMed: 22743772]

Seymour PA, Freude KK, Tran MN, Mayes EE, Jensen J, Kist R, Scherer G, and Sander M (2007). SOX9 is required for maintenance of the pancreatic progenitor cell pool. Proc. Natl. Acad. Sci. USA 104, 1865–1870. [PubMed: 17267606]

Shinoda G, Shyh-Chang N, Soysa TY, Zhu H, Seligson MT, Shah SP, Abo-Sido N, Yabuuchi A, Hagan JP, Gregory RI, et al. (2013). Fetal deficiency of lin28 programs life-long aberrations in growth and glucose metabolism. Stem Cells 31, 1563–1573. [PubMed: 23666760]

Shyh-Chang N, and Daley GQ (2013). Lin28: primal regulator of growth and metabolism in stem cells. Cell Stem Cell 12, 395–406. [PubMed: 23561442]

Singh I, Mehta A, Contreras A, Boettger T, Carraro G, Wheeler M, Cabrera-Fuentes HA, Bellusci S, Seeger W, Braun T, and Barreto G (2014). Hmga2 is required for canonical WNT signaling during lung development. BMC Biol. 12, 21. [PubMed: 24661562]

Tan SM, Altschuler G, Zhao TY, Ang HS, Yang H, Lim B, Vardy L, Hide W, Thomson AM, and Lareu RR (2014). Divergent LIN28-mRNA associations result in translational suppression upon the initiation of differentiation. Nucleic Acids Res. 42, 7997–8007. [PubMed: 24860167]

Tan FE, Sathe S, Wheeler EC, Nussbacher JK, Peter S, and Yeo GW (2019). A Transcriptome-wide Translational Program Defined by LIN28B Expression Level. Mol. Cell 73, 304–313.e3. [PubMed: 30527666]

Taniguchi H, He M, Wu P, Kim S, Paik R, Sugino K, Kvitsiani D, Fu Y, Lu J, Lin Y, et al. (2011). A resource of Cre driver lines for genetic targeting of GABAergic neurons in cerebral cortex. Neuron 71, 995–1013. [PubMed: 21943598]

Tompkins DH, Besnard V, Lange AW, Wert SE, Keiser AR, Smith AN, Lang R, and Whitsett JA (2009). Sox2 is required for maintenance and differentiation of bronchiolar Clara, ciliated, and goblet cells. PLoS One 4, e8248. [PubMed: 20011520]

Tsialikas J, and Romer-Seibert J (2015). LIN28: roles and regulation in development and beyond. Development 142, 2397–2404. [PubMed: 26199409]

Tu HC, Schwitalla S, Qian Z, LaPier GS, Yermalovich A, Ku YC, Chen SC, Viswanathan SR, Zhu H, Nishihara R, et al. (2015). LIN28 cooperates with WNT signaling to drive invasive intestinal and colorectal adenocarcinoma in mice and humans. Genes Dev. 29, 1074–1086. [PubMed: 25956904]

Urbach A, Yermalovich A, Zhang J, Spina CS, Zhu H, Perez-Atayde AR, Shukrun R, Charlton J, Sebire N, Mifsud W, et al. (2014). Lin28 sustains early renal progenitors and induces Wilms tumor. Genes Dev. 28, 971–982. [PubMed: 24732380]

Vadla B, Kemper K, Alaimo J, Heine C, and Moss EG (2012). lin-28 controls the succession of cell fate choices via two distinct activities. PLoS Genet. 8, e1002588. [PubMed: 22457637]

Viswanathan SR, Daley GQ, and Gregory RI (2008). Selective blockade of microRNA processing by Lin28. Science 320, 97–100. [PubMed: 18292307]

Viswanathan SR, Powers JT, Einhorn W, Hoshida Y, Ng TL, Toffanin S, O'Sullivan M, Lu J, Phillips LA, Lockhart VL, et al. (2009). Lin28 promotes transformation and is associated with advanced human malignancies. Nat. Genet 41, 843–848. [PubMed: 19483683]

Wan H, Dingle S, Xu Y, Besnard V, Kaestner KH, Ang SL, Wert S, Stahlman MT, and Whitsett JA (2005). Compensatory roles of Foxa1 and Foxa2 during lung morphogenesis. J. Biol. Chem 280, 13809–13816. [PubMed: 15668254]

West JA, Viswanathan SR, Yabuuchi A, Cunniff K, Takeuchi A, Park IH, Sero JE, Zhu H, Perez-Atayde A, Frazier AL, et al. (2009). A role for Lin28 in primordial germ-cell development and germ-cell malignancy. Nature 460, 909–913. [PubMed: 19578360]

Wilbert ML, Huelga SC, Kapeli K, Stark TJ, Liang TY, Chen SX, Yan BY, Nathanson JL, Hutt KR, Lovci MT, et al. (2012). LIN28 binds messenger RNAs at GGAGA motifs and regulates splicing factor abundance. Mol. Cell 48, 195–206. [PubMed: 22959275]

Xu B, Zhang K, and Huang Y (2009). Lin28 modulates cell growth and associates with a subset of cell cycle regulator mRNAs in mouse embryonic stem cells. RNA 15, 357–361. [PubMed: 19147696]

Yang DH, and Moss EG (2003). Temporally regulated expression of Lin-28 in diverse tissues of the developing mouse. Gene Expr. Patterns 3, 719–726. [PubMed: 14643679]

Yermalovich AV, Osborne JK, Sousa P, Han A, Kinney MA, Chen MJ, Robinton DA, Montie H, Pearson DS, Wilson SB, et al. (2019). Lin28 and let-7 regulate the timing of cessation of murine nephrogenesis. Nat. Commun 10, 168. [PubMed: 30635573]

Zhu H, Shah S, Shyh-Chang N, Shinoda G, Einhorn WS, Viswanathan SR, Takeuchi A, Grasemann C, Rinn JL, Lopez MF, et al. (2010). Lin28a transgenic mice manifest size and puberty phenotypes identified in human genetic association studies. Nat. Genet 42, 626–630. [PubMed: 20512147]

Zhu H, Shyh-Chang N, Segrè AV, Shinoda G, Shah SP, Einhorn WS, Takeuchi A, Engreitz JM, Hagan JP, Kharas MG, et al.; DIAGRAM Consortium; MAGIC Investigators (2011). The Lin28/let-7 axis regulates glucose metabolism. Cell 147, 81–94. [PubMed: 21962509]

Highlights

- Lin28a and Lin28b control the timing of branching morphogenesis
- Mature *Let-7* family members are not highly expressed until mid-gestation in lung
- Lin28a binds and controls expression of *Sox2*, *Sox9*, and *Etv5* mRNA

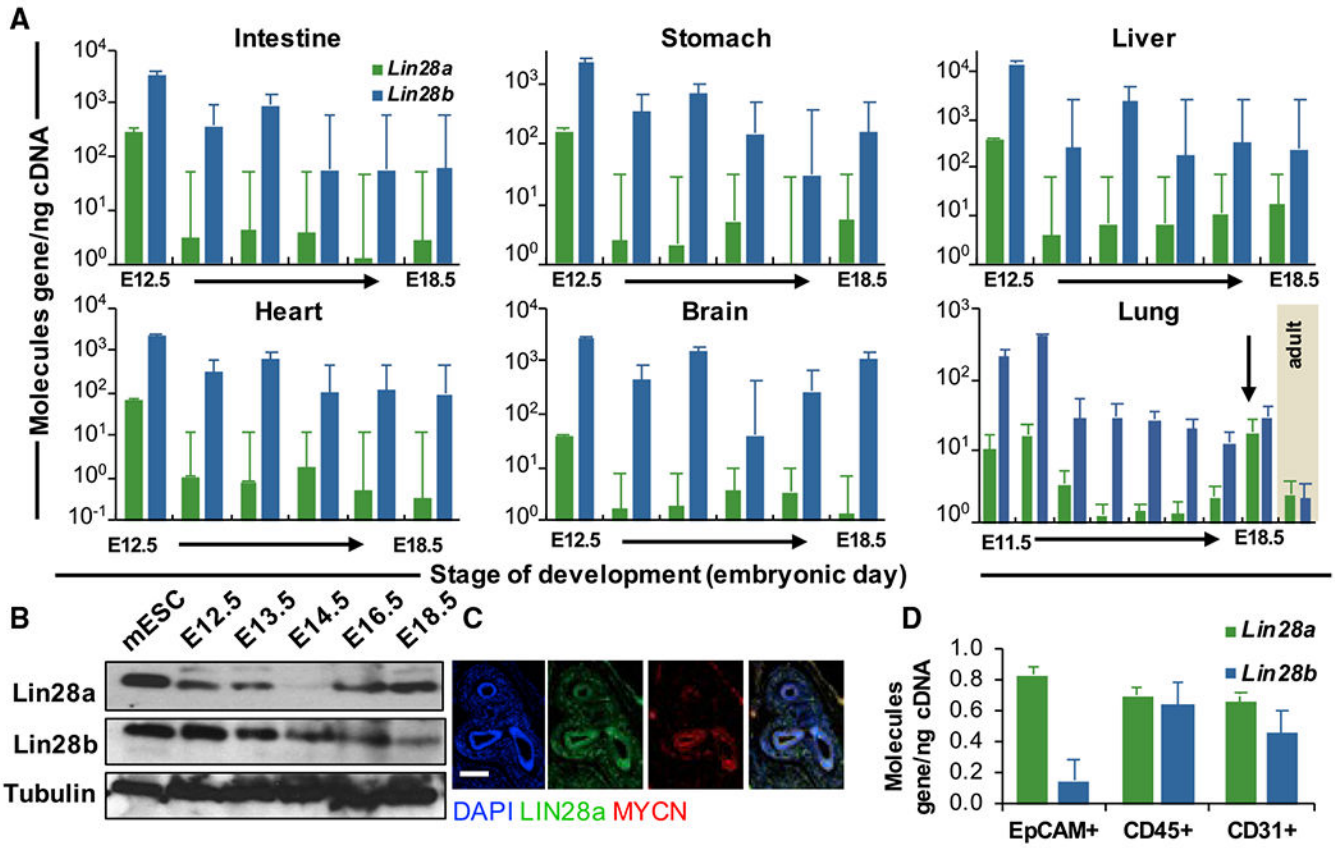

Figure 1. Expression of *Lin28a* and *Lin28b* in the whole embryo and mouse lung

(A) qRT-PCR was conducted on two independent cohorts of the intestine, stomach, liver, heart, and brain from ages E12.5 to E18.5 (minus E16.5) and on three cohorts of lungs from ages E11.5 to adult by using DNA standards designed to amplify exon 2 for *Lin28a* and *Lin28b*. Error bars represent technical replicates of two independant biological samples for intestine, staomach, liver, heart, brain. Error bars represent biological replicates of three independant biological samples for lung

(B) Immunoblots for protein expression were done with one of three cohorts of lung mentioned above from ages E12.5 to E18.5 by using mESCs as the control, conducted for Lin28a, Lin28b, and tubulin.

(C) Immunofluorescence was conducted on an E11.5 wild-type (WT) frozen lung section for Lin28a, MynN, and DAPI.

(D) We conducted qRT-PCR for *Lin28a* and *Lin28b* by using standards that amplify exon 2 of *Lin28a* and *Lin28b* from sorted lung fractions, n = 3 at E12.5. Error bars represent biological replicates of three independant biological samples. Scale bar, 0.5 mm.

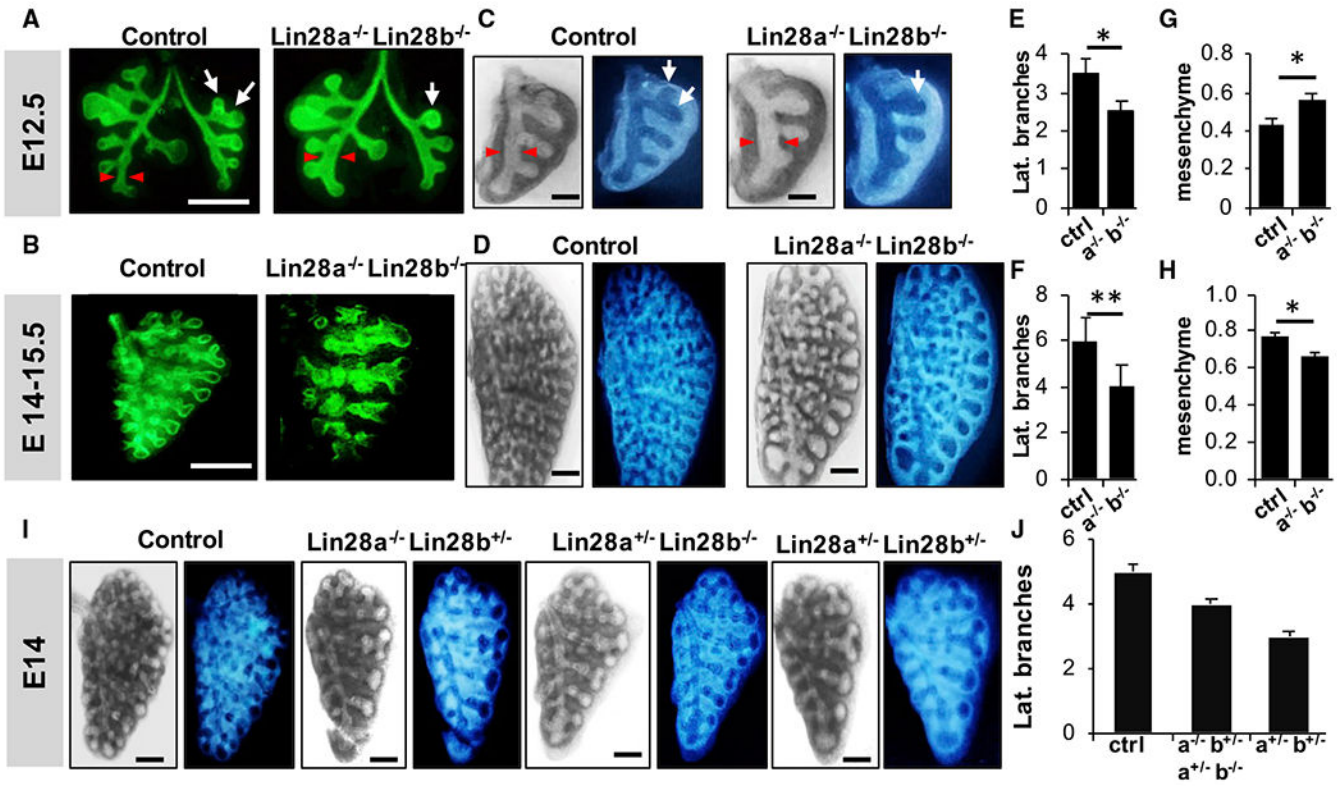

Figure 2. Loss of *Lin28a* and *Lin28b* leads to aberrant lung branching morphogenesis

(A and B) Whole-mount immunostaining in control (without *NKX2.1*^{creER} allele) and double *Lin28a* and *Lin28b* knockout (*d*KO) lungs at E12.5 (A) and E14.0 (B); lungs were stained for E-cadherin to show the epithelium. Tamoxifen was injected at E10.5. White arrows point to specific differences in the branch pattern of the cranial most lateral secondary branch in left lobe (L.L1) and the L.L1.A1 branch that did not formed in the mutant lung. Right: Red arrows denote abnormalities in bronchi size.

(C and D) Whole left lungs imaged in brightfield together with images in negative-contrast channels to show distinction of the mesenchyme in control and *d*KO lungs at E12.5 (C) and E15.5 (D). The n = 30 of all time points examined (E12.5, E13.0, E14.0, E15.5, and E18.5) of the double knockouts with abnormal phenotype for the *d*KO compared to the control (no cre, littermates); n = 34 across 11 litters.

(E and F) Graphs quantifying lateral secondary branches of a subset of E12.5 and E15.5 lungs from different litters; E12.5, n = 4 lungs from 3 different litters, *$p < 0.05$ (E); E15.5, n = 4 lungs from 2 different litters, **$p < 0.01$ (F). All controls are littermates.

(G and H) Graphs quantifying area of mesenchyme at E12.5 and E15.5 compared to whole lung area; E12.5, n = 7 lungs from 2 different litters (G); E15.5, n = 6,3 lungs in Figure S2F (H).

(I) Whole left lungs imaged in brightfield (left to right) from control, Lin28a$^{-/-}$Lin28b$^{+/-+/-}$*;NKX2.1creER*, Lin28a$^{+/-}$Lin28b$^{+/-+/-}$*;NKX2.1creER*, and Lin28a$^{+/-}$Lin28b$^{-/-+/-}$*;NKX2.1creER*.

(J) Graph quantifying the number of lateral branches in (I); n = 2 lungs from 2 different controls, Lin28a$^{-/-}$Lin28b$^{+/-}$*; NKX2.1creER*, and Lin28a$^{+/-}$Lin28b$^{-/-}$*; NKX2.1creER*; and n =

3 lungs from 2 different litters for Lin28a$^{+/-}$Lin28b$^{+/-}$*NKX2.1creER*. Statistics for double knockouts were calculated by one-way ANOVA. All scale bars, 0.5 mm.

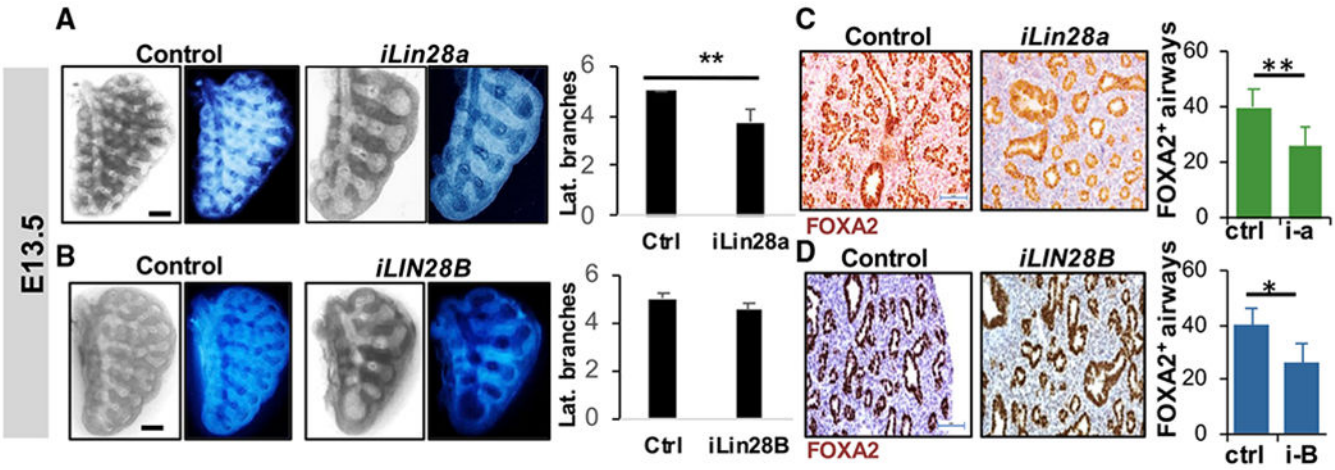

Figure 3. Gain of Lin28a or LIN28B leads to aberrant lung branching morphogenesis

(A and B) Left: Whole left lungs imaged in brightfield together with images in negative-contrast channels to show contrast for mesenchyme in control and inducible LIN28 (*iLin28a*: *Nkx2.1CreER* or *iLIN28B*: *Nkx2.1CreER*). (A) The mouse *Lin28a* gene. (B) The human *LIN28B* gene. Genes induced by the addition of doxycycline and tamoxifen at E10.5. Right: Graphs quantifying the number of lateral branches in left panels; n = 3 lungs from control, *iLin28a*, and *iLIN28B*; *p < 0.05, **p < 0.01. Statistics for knockout were calculated by one-way ANOVA.

(C and D) Mouse (C) and human (D). Left panels: Sections of lungs at E13.5 stained by immunohistochemistry for the epithelial marker FOXA2. Right panel: Graphs quantifying number of Foxa2+ airways in the left panel *p = 0.05, **p = 0.01. Analyses of stats for inducible data used one-way ANOVA. Scale bar, 0.5 mm for (A) and (B). Scale bars for (C) and (D), 50 μm.

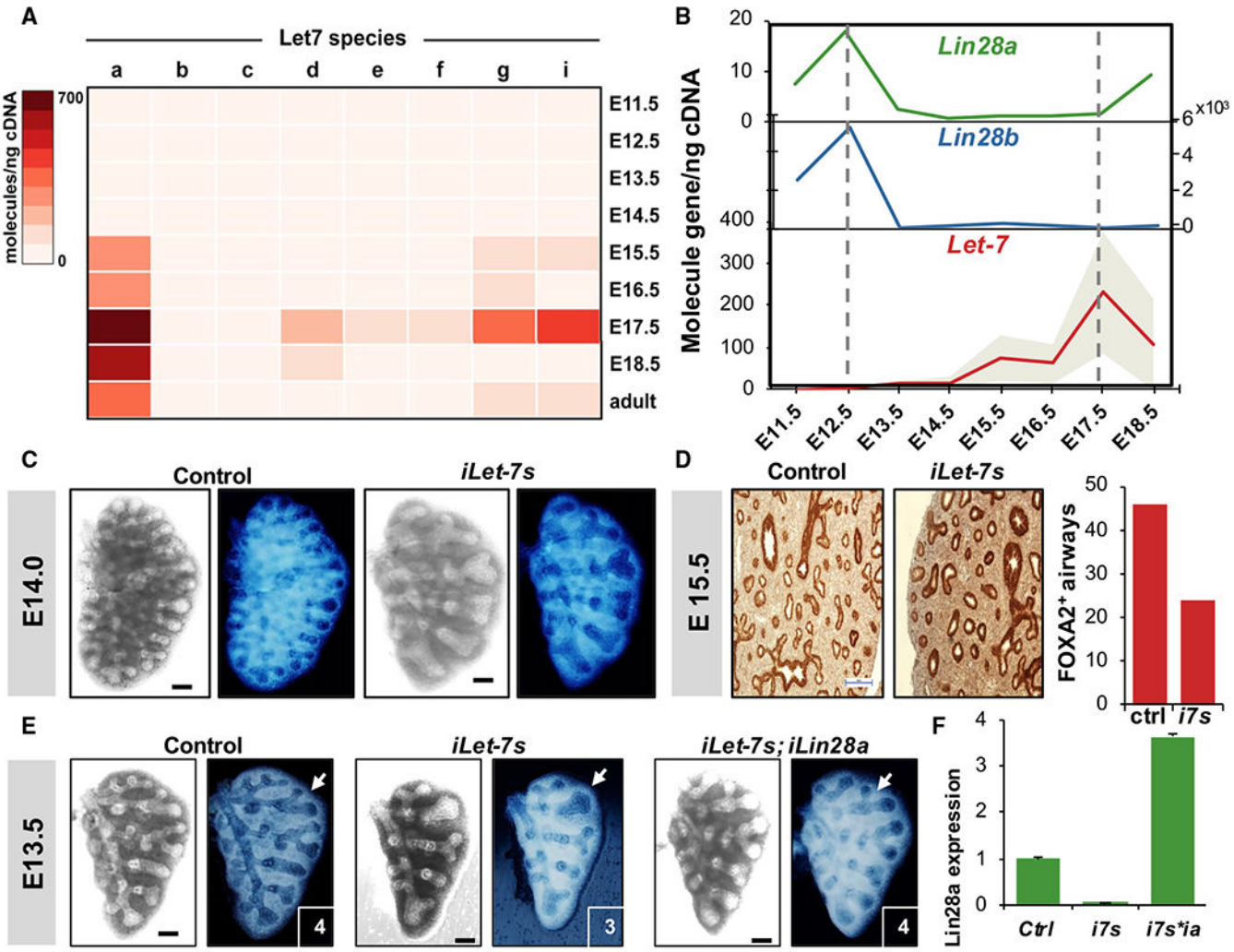

Figure 4. Mature *let-7* is not expressed during early lung development but is sufficient to impair branching morphogenesis by regulation of *Lin28*

(A) Heatmap representing qRT-PCR conducted on two cohorts of lungs for quantitative analysis of all *let-7* family members.

(B) Graph of absolute expression levels of *Lin28a, Lin28b*, and all *let-7* family members across lung development.

(C) Whole left lungs were imaged in bright field together with images in negative-contrast channels to show contrast for mesenchyme in control and inducible *let-7S21L;* $^{Nkx2.1CreER}$ at E14.0.

(D) Left: Sections of lungs at E15.5 immunostained by using immunohistochemistry for the epithelial marker FoxA2. Right: Quantification of the FoxA2+ airways in the right panel. Scale bar, 0.5 mm.

(E) Whole left lungs imaged in bright field together with images in negative-contrast channels to show contrast for mesenchyme in control (left panel), inducible *let-7S21L* (middle panel), and inducible *let-7S21L* together with inducible *Lin28a* (right panel) at E13.5. White number indicates lateral branches, and white arrows point to rescue of an individual branching defect.

(F) *Lin28a* expression in lungs from the control (left panel), inducible *let-7 S21L* (*let-7S21L*; middle panel), and inducible *let-7S21L* together with inducible *iLin28a*; *Nkx2.1CreER* (right panel) from (E). Scale bars, 0.5 mm for (C) and (E). Scale bars, 50 μm for (D).

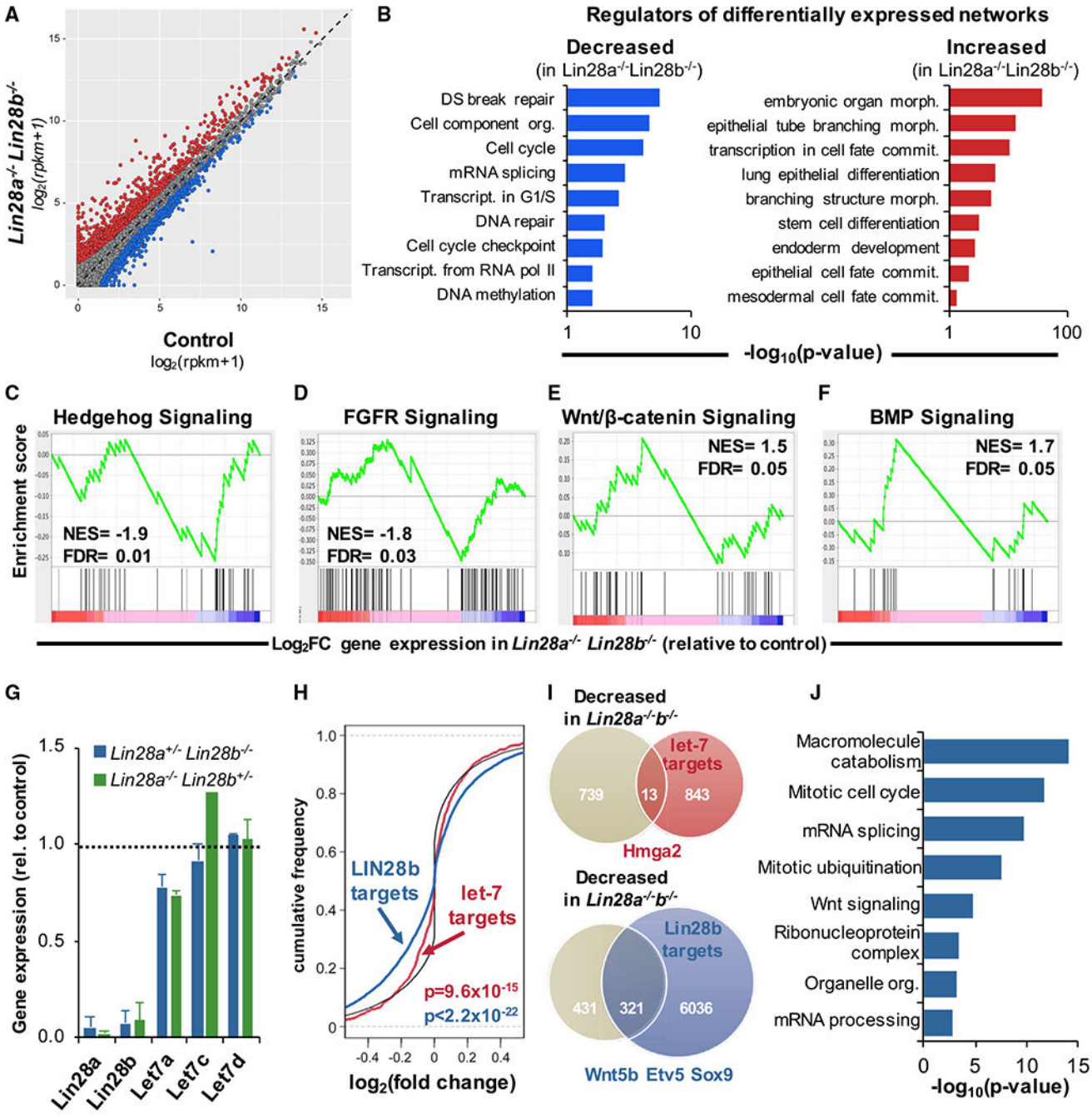

Figure 5. Lin28a/b regulate pathways involved in branching morphogenesis

(A) RNA-seq on control and *d*KO whole lungs at E12.5. The plot represents global gene expression levels.

(B) Gene regulatory networks that were differentially expressed in the RNA-seq were identified using CellNet framework (Cahan et al., 2014). Enriched transcription factors were then further annotated using Gene Ontology (GO) terminology.

(C–F) Gene set enrichment analysis (GSEA) of pathways changed relative to the WT.

(G) RT-qPCR was conducted on *Lin28a*$^{+/-}$ *Lin28b*$^{-/-;}$ *NKX2.1creER* and *Lin28a*$^{-/-}$ *Lin28b*$^{+/-}$; *NKX2.1creER* whole lungs for the expression of *Lin28a* and *Lin28b* and *let-7a*, *let-7c*, and *let-7d* at E12.5.

(H) Cumulative distribution function of mRNA changes for *let-7* targets (predicted from Target Scan) and reported physical Lin28b targets (CLIP-sequencing) (Madison et al., 2013).

(I) Venn diagram of differential genes (>1.5-fold downregulated) identified for all 856 predicted *let-7* targets, of which 13 genes were changed (1.7% overlap; $p = 0.002$ for depletion), and 6,357 physical targets of Lin28b, of which 321 were changed ($p = 1.3 \times 10^{-12}$ for over-representation).

(J) Significant GO terms that were enriched in the differential CLIP targets of Lin28b.

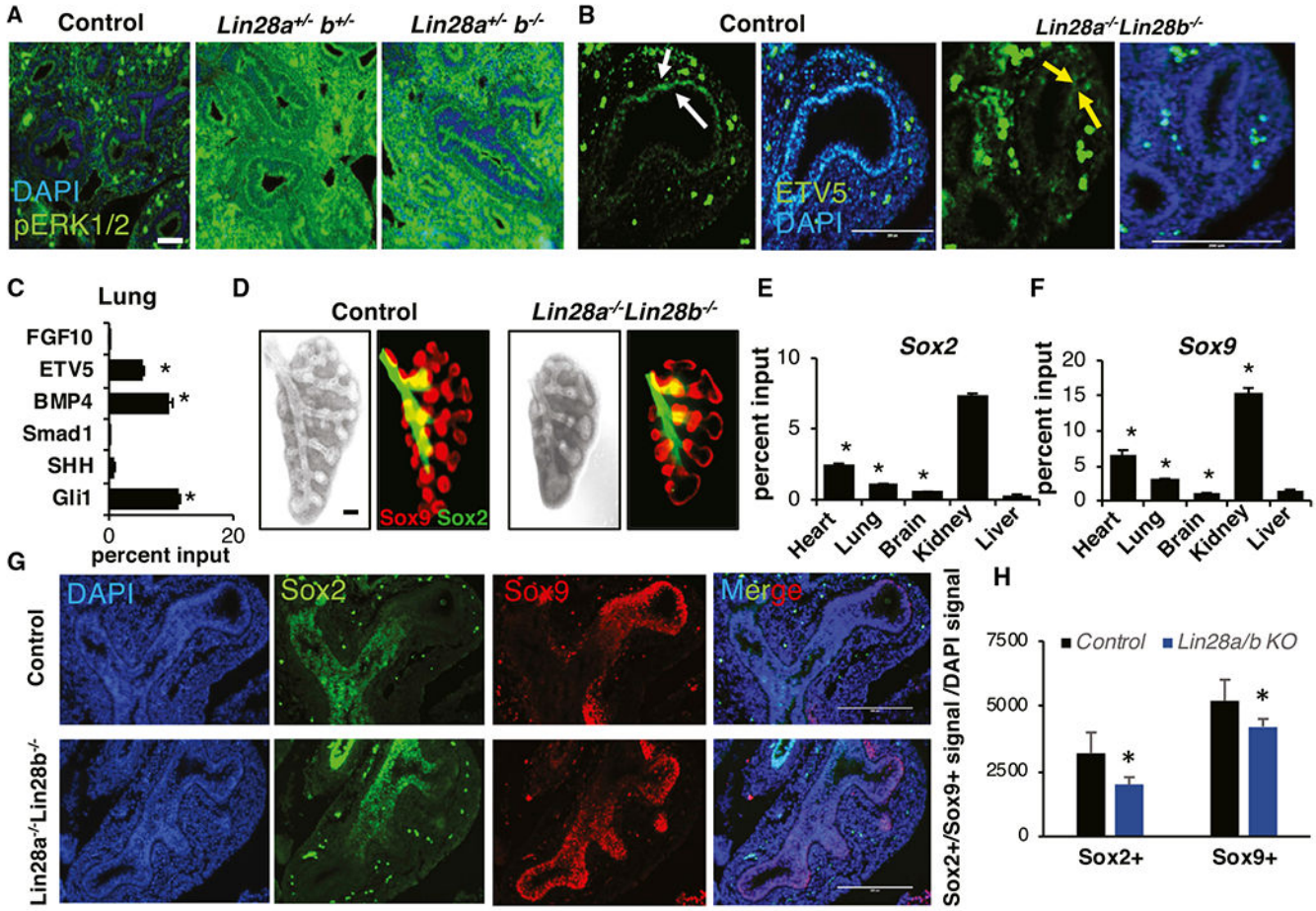

Figure 6. Lin28a and Lin28b coordinate feedback loops between SHH/FGF10

(A and B) Immunofluorescence for phosphorylated ERK (pERK) at E14.0 (A) and ETV5 at E12.5 (B) from sectioned control and *Lin28a/b*-deficient lungs $Lin28a^{+/-}b^{+/-;NKX2.1creER}$, $Lin28a^{+/-}b^{-/-;NKX2.1creER}$, and $Lin28a^{-/-}b^{-/-;NKX2.1creER}$.

(C) RNA immunoprecipitation (RIP) using antibodies against Lin28a. RIPs were done in WT CD1 mice from E13.0 lung. RT-PCR was done from mRNAs bound to LIN28 (all within coding regions) of *Etv5*, *Fgf10*, *Bmp4*, *Smad1*; and *Shh*, *Gli1*. The analysis is represented as percentage of input. *p < 0.05 compared to immunoglobulin G (IgG).

(D) Right: Brightfield images of whole left lungs from control and $Lin28a^{-/-}/Lin28b^{-/-;\ NKX2.1creER}$ lungs Left: Whole-mount lung immunostaining done for control and $Lin28a^{-/-}/Lin28b^{-/-;\ NKX2.1creER}$ lungs at E13.5 stained for Sox2 and Sox9 to show proximal and distal epithelium.

(E and F) RIP using antibodies against Lin28a. RIPs were done in WT CD1 mice from E13.0 heart, lung, brain, kidney, and liver. RT-PCR was done from mRNAs bound to LIN28 (within coding regions) of *Sox2* (E) and *Sox9* (F). The analysis is represented as percentage to input. *p < 0.05 compared to IgG by t test.

(G) Representative images of immunofluorescence for Sox2, Sox9, and DAPI at E12.5 from sectioned control and $Lin28a^{-/-}Lin28b^{-/-;NKX2.1creER}$ lungs.

(H) Quantification of immunofluorescence from (G), for Sox2 and Sox9 at E12.5 from sectioned control and *Lin28a*$^{-/-}$ *Lin28b*$^{-/-}$;*NKX2.1creER* lungs. A total of 12 slices from each sample was used to quantify either Sox2 or Sox9 positivity per cell (as measured by DAPI). *$p < 0.05$. Scale bars, 0.5 mm for (A(and (D); scale bars, 200 μm for (B) and (G).

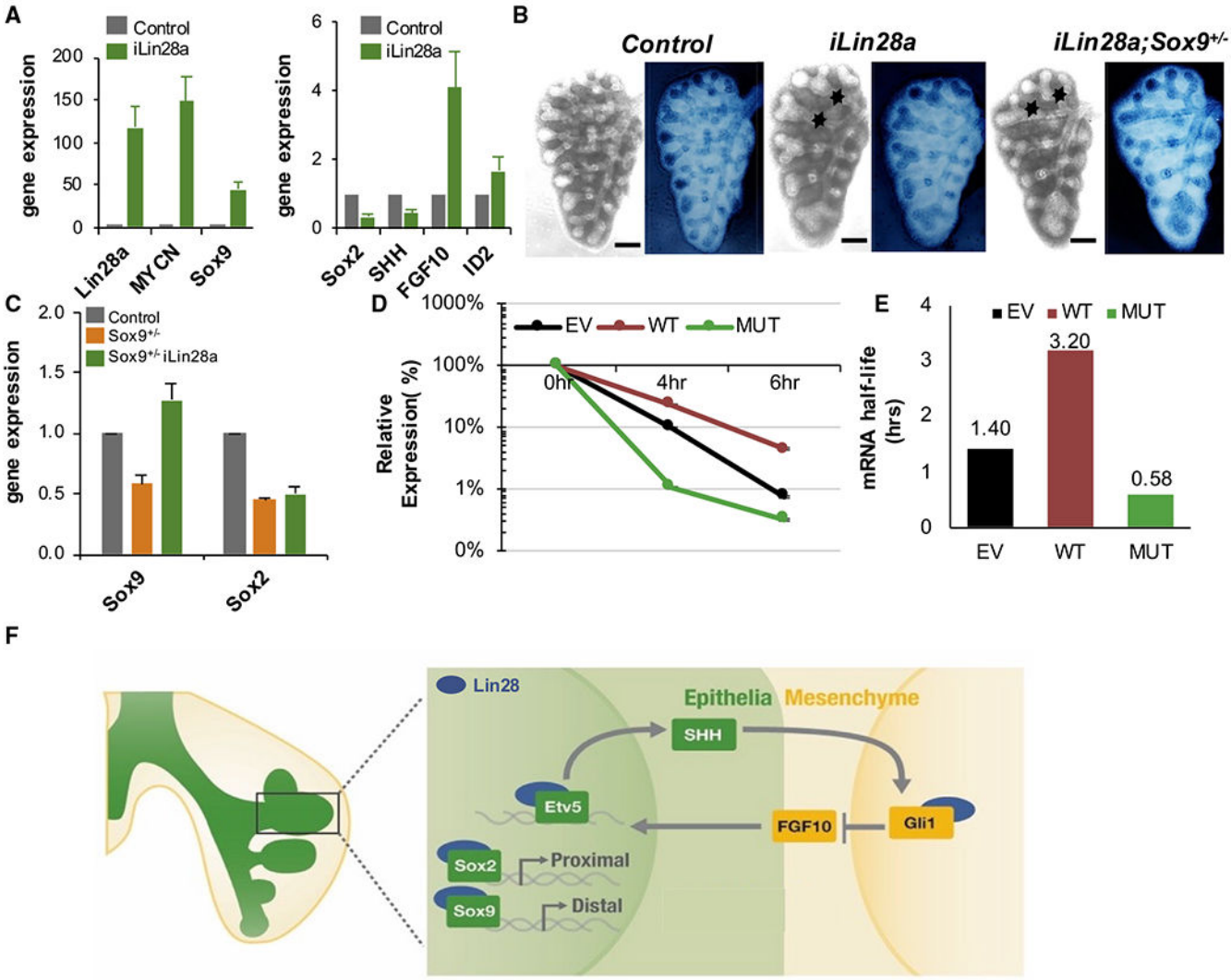

Figure 7. Lin28a regulates expression of *Sox9*

(A) Relative qRT-PCR done for *Lin28a*, *Nmyc*, *Sox2*, *SHH*, *FGF10*, *ID2*, and *Sox9* mRNA from control and inducible Lin28a (*iLin28a*$^{NKX2.1creER}$) lungs. Tamoxifen and doxycycline were added at E10.5; lungs were dissected at E13.5.

(B) Whole left lungs imaged in brightfield together with images in negative-contrast channels to show contrast for mesenchyme in control, inducible Lin28 (*iLin28a*$^{NKX2.1creER}$), and inducible Lin28a together with heterozygous loss of Sox9 (*iLin28a; Sox9*$^{+/-;\ NKX2.1creER}$). Tamoxifen was injected at E10.5, and mice were sacrificed at E14; control and i*Lin28a*, n = 4 lungs from 2 different litters; i*Lin28a; Sox9*$^{+/-}$, n = 3 from 2 different litters.

(C) Relative qRT-PCR done for *Sox9* and *Sox2* from control, *Sox9*$^{+/-;\ NKX2.1creER}$, and i*Lin28a; Sox9*$^{+/-;\ NKX2.1creER}$.

(D) Relative qRT-PCR was done of HEK293 cells expressing GFP (control), WT LIN28A, or an RNA-binding mutant (MUT) LIN28A that was then treated with actinomycin D for 0, 4, or 6 h. Representative plot of n = 4 experiments.

(E) Measurements of mRNA half-life following qRT-PCR for data in (D).

(F) Model of LIN28 binding to transcriptions factors *Sox2*, *Sox9*, and *Etv5* in the epithelia and *Gli1* in mesenchyme. Scale bars, 0.5 mm.

KEY RESOURCES TABLE

REAGENT or RESOURCE	SOURCE	IDENTIFIER
Antibodies		
PE anti-mouse CD31	BioLegend	cat#102508; RRID:AB_312915
PerCP-Cy5.5 anti-mouse CD45	eBioscience	cat#103132; RRID:AB_469717
PECy7 anti-mouse EpCAM	BioLegend	cat #118216; RRID:AB_1236471
anti-rabbit Lin28a	Cell Signaling	#A177 RRID AB_2297060
anti-mouse specific Lin28b	Cell Signaling	cat#5422S; RRID:AB_10697489
anti-rabbit α/β tubulin	Cell Signaling	cat#2148S
anti-mouse Ecadherin	Novex (Life Technologies)	Clone: ECCD2 Cat#13-1900
anti-goat SOX2	Santa Cruz (Discontinued)	cat#SC-17320 ; RRID AB_2286684
anti-rabbit SOX9	Millipore	cat#AB5535; RRID AB_2239761
anti-rabbit LIN28 (used for IP)	Abcam	cat#ab63740 and #ab46020
anti-rabbit IgG (used for IP)	Santa Cruz	cat# SC-2491; RRID:AB_628495
AP conjugate anti-sheep digoxigenin	Roche	cat#50-100-3276; RRID:AB_514497
Chemicals, peptides, and recombinant proteins		
Tamoxifen	Sigma	cat# T5648
Doxycycline	Sigma	cat#D9891
Collagenase/Dispase	Roche	cat#1026963
TRIzol	Life Technologies	cat#15596026
RNaseOUT inhibitor	Invitrogen	cat#10777019
Actinomycin D	Sigma	cat# A9415
RIPA buffer	Sigma	cat#R0278
Halt-Protease and Phosphatase Cocktail in	Thermo Scientific	cat# 78442
OCT freezing medium	Tissue-Tek	cat#4583
Donkey Serum	Sigma	cat#D9663
Critical commercial assays		
SMARTer ULTRA Low Input RNA Kit	Clonetech	cat#634936
miSCRIPT II RT Kit	QIAGEN	cat#/ID: #218161
T7 *in vitro* transcription Kit	Life Technologies	cat#AM1333
DAB Substrate	Vector Labs	cat# SK-4100
Deposited data		
RNA-seq	This manuscript	GEO: GSE93571
LIN28B Clip-Seq	Madison et al., 2013	N/A
Experimental models: Cell lines		
HEK293	Sigma	cat#85120602
Experimental models: Organisms/strains		
Wild Type, CD-1mice	Charles River	Crl:CD1(ICR)
Col1a-TRE-Lin28a mice	N/A	Zhu et al., 2010

REAGENT or RESOURCE	SOURCE	IDENTIFIER
Col1a-TRE-LIN28B mice	N/A	Zhu et al., 2011
Col1a-TRE- let-7S21L mice	N/A	Zhu et al., 2011
Lin28b$^{fl/fl}$ mice	N/A	Shinoda et al., 2013
Lin28a$^{fl/fl}$ mice	N/A	Shinoda et al., 2013
Nkx2.1creER mice	Jackson Laboratories	no. 014552
Sox9$^{fl/fl}$ mice	Jackson Laboratories	no. 013106
Lox-stop-LoxTdtomato	Jackson Laboratories	no. 007914
Ddx4-cre	Jackson Laboratories	no. 006954
Oligonucleotides		
See Table S2 for Primer Sequences and catalog numbers		N/A
Recombinant DNA		
a human pBABE-LIN28A mutant	This Manuscript	N/A; available upon request from Lead Contact
human pBabe-LIN28A wildtype	This Manuscript	N/A; available upon request from Lead Contact
human pBabe-GFP	This manuscript	N/A; available upon request from Lead Contact
Software and algorithms		
GraphPad Prism 7	GraphPad	https://www.graphpad.com/scientific-software/prism/
ImageJ (Fuji)	https://imagej.net/software/fiji	Schindelin et al., 2012
TopHat2	Kim et al., 2013	N/A
CellNet	https://github.com/pcahan1/CellNet_Cloud	Cahan et al., 2014
TargetScan	Agarwal et al., 2015	N/A